Endothelium-derived semaphorin 3G attenuates ischemic retinopathy by coordinating β-catenin–dependent vascular remodeling

Dan-Yang Chen,[1,2,3] Ning-He Sun,[1,2,3] Xiang Chen,[2] Jun-Jie Gong,[2] Song-Tao Yuan,[4] Zi-Zhong Hu,[4] Nan-Nan Lu,[3] Jakob Körbelin,[5] Kohji Fukunaga,[6] Qing-Huai Liu,[4] Ying-Mei Lu,[1] and Feng Han[2,7]

[1]Department of Physiology, School of Basic Medical Sciences, Nanjing Medical University, Nanjing, China. [2]Key Laboratory of Cardiovascular & Cerebrovascular Medicine, Drug Target and Drug Discovery Center, School of Pharmacy, Nanjing Medical University, Nanjing, China. [3]Institute of Pharmacology and Toxicology, College of Pharmaceutical Sciences, Zhejiang University, Hangzhou, China. [4]Department of Ophthalmology, the First Affiliated Hospital of Nanjing Medical University, Nanjing, China. [5]Department of Oncology and Hematology, University Medical Center Hamburg-Eppendorf, Hamburg, Germany. [6]Department of Pharmacology, Graduate School of Pharmaceutical Sciences, Tohoku University, Sendai, Japan. [7]Institute of Brain Science, the Affiliated Brain Hospital of Nanjing Medical University, Nanjing, China.

Abnormal angiogenesis and regression of the diseased retinal vasculature are key processes associated with ischemic retinopathies, but the underlying mechanisms that regulate vascular remodeling remain poorly understood. Here, we confirmed the specific expression of semaphorin 3G (Sema3G) in retinal endothelial cells (ECs), which was required for vascular remodeling and the amelioration of ischemic retinopathy. We found that Sema3G was elevated in the vitreous fluid of patients with proliferative diabetic retinopathy (PDR) and in the neovascularization regression phase of oxygen-induced retinopathy (OIR). Endothelial-specific *Sema3G* knockout mice exhibited decreased vessel density and excessive matrix deposition in the retinal vasculature. Moreover, loss of *Sema3G* aggravated pathological angiogenesis in mice with OIR. Mechanistically, we demonstrated that HIF-2α directly regulated *Sema3G* transcription in ECs under hypoxia. Sema3G coordinated the functional interaction between β-catenin and VE-cadherin by increasing β-catenin stability in the endothelium through the neuropilin-2 (Nrp2)/PlexinD1 receptor. Furthermore, Sema3G supplementation enhanced healthy vascular network formation and promoted diseased vasculature regression during blood vessel remodeling. Overall, we deciphered the endothelium-derived Sema3G-dependent events involved in modulating physiological vascular remodeling and regression of pathological blood vessels for reparative vascular regeneration. Our findings shed light on the protective effect of Sema3G in ischemic retinopathies.

Introduction

Functional vascular networks in the retina are formed by sprouting during angiogenesis. They subsequently undergo vascular remodeling, which is characterized by precise vascular pruning to construct mature vasculature (1). Excessive vascular pruning is accompanied by the destruction of barrier function and damage to the local tissue microenvironment (2). A number of diseases are caused by perturbed microvascular remodeling and aberrant functional vessel recovery. Proliferative diabetic retinopathy (PDR) and retinopathy of prematurity (ROP) are the most common types of retinal ischemia-induced proliferative retinopathies (3, 4). These disorders involve initial microvascular degeneration and insufficient vascular network formation, resulting in pathological neovascularization as a compensatory response (3, 4). A large increase in the expression of vascular endothelial growth factor (VEGF) contributes to neovascularization in retinopathy (5). Intravitreal therapy with anti-VEGF neutralizing antibodies is a key treatment for these retinal vascular diseases in the clinic (6). However, some patients with vascular diseases are refractory to anti-VEGF therapy (7). Thus, it is important to elucidate the mechanisms that initiate and promote vascular changes in pathological angiogenesis, especially mediating spontaneous regression and normalization of pathological retinal vessels. Understanding these mechanisms will enable the development of new strategies to restore normal vessels.

Growing evidence indicates that angiogenesis is coordinated by guidance molecules during vascular development (8, 9). Semaphorin signaling is widely implicated in physiological and pathological processes of the vascular system (10). Class 3 semaphorins (Sema3s) are secreted proteins that mainly function through a receptor complex in which neuropilins associate with plexins. Plexins modulate the activity of GTPases and regulate downstream kinase activity as signal transducing elements (10). Semaphorin 3G (Sema3G) is expressed specifically in endothelial cells (ECs) and belongs to the subfamily of class 3 secreted semaphorins (11). Previous studies have indicated that Sema3G conditional knockout mice exhibit impaired hippocampus-dependent

Authorship note: DYC and NHS contributed equally to this work and are co–first authors.
Conflict of interest: The authors have declared that no conflict of interest exists.

Submitted: November 27, 2019; **Accepted:** December 10, 2020;
Published: February 15, 2021.
Reference information: *J Clin Invest*. 2021;131(4):e135296.
https://doi.org/10.1172/JCI135296.

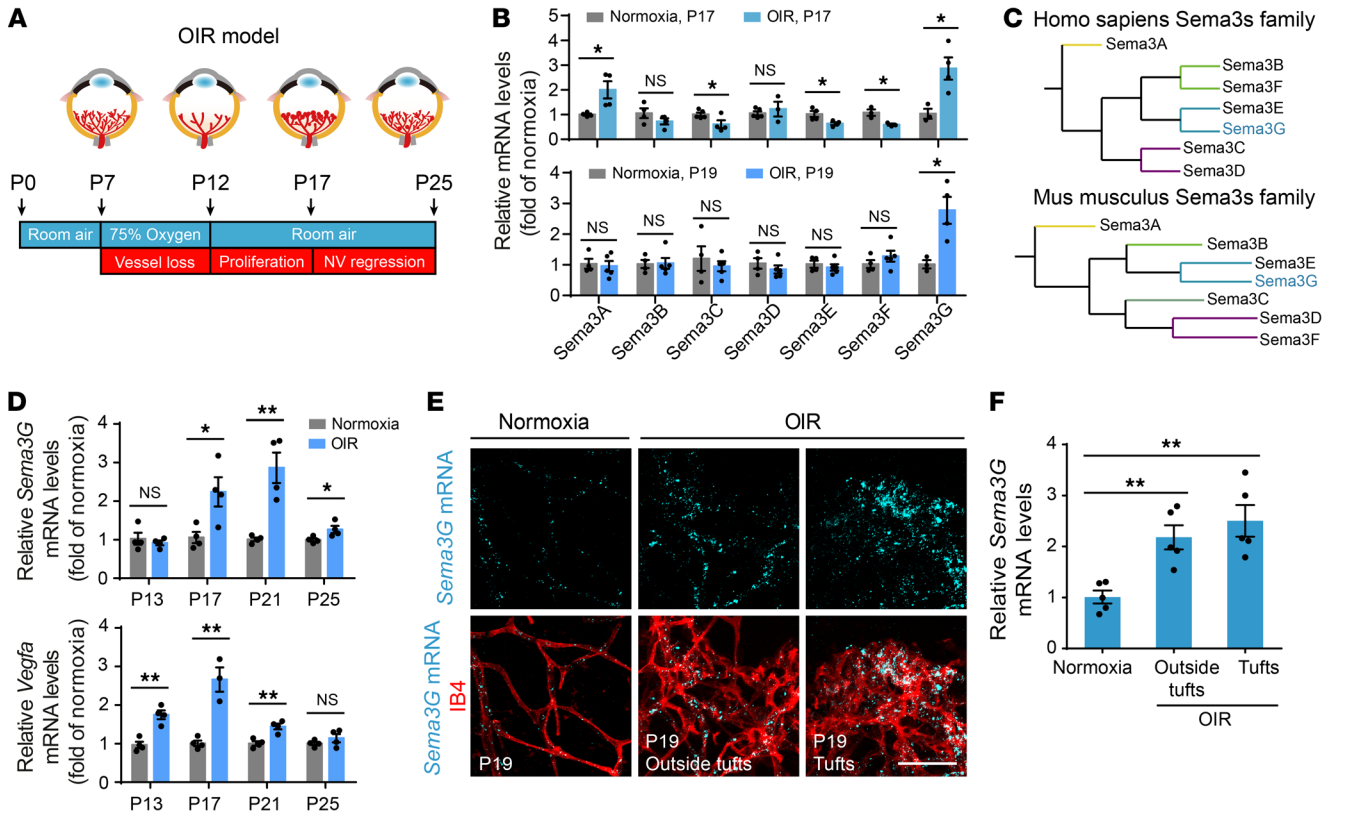

Figure 1. Sema3G is elevated in the retinas of mice in the OIR model. (**A**) Schematic illustration of the mouse oxygen-induced retinopathy (OIR) model. (**B**) RT-qPCR analysis of *Sema3s* mRNA in normoxic or OIR retinas at P17 and P19. Data were normalized to gene mRNA expression upon normoxia (n = 3–5 mice). (**C**) The evolutionary relationship of Sema3s among human or mouse species. (**D**) RT-qPCR analysis of *Sema3G* and *Vegfa* mRNA in the retina at the times indicated. Data were normalized to gene mRNA expression upon normoxia (n = 3–4 mice for each group). (**E** and **F**) Localization and quantification of *Sema3G* mRNA in whole-mount retinas upon normoxia and OIR at P19 (n = 5 mice for each group). Error bars represent mean ± SEM, $^*P < 0.05$; $^{**}P < 0.01$; 2-tailed Student's t tests. Scale bar: 50 μm (**E**). NV, neovascularization.

memory and reduced spine density (12). Peripheral Sema3G regulates the differentiation of adipocytes and is associated with obesity (13). In pathological states, Sema3G can function as a potent antitumorigenic agent by exerting antiinvasion activity in tumor cells and reducing the density of tumor-associated blood vessels (14–16). Sema3G has also been found to be a significant prognostic marker in adult gliomas (14) and it binds to neuropilin-2 (Nrp2) in vitro (11, 17, 18). To date, however, the essential in vivo role of Sema3G in vascular development and pathology, especially its intracellular signaling in ischemic retinopathy, remains unclear.

Here, we show that knockout of *Sema3G* in ECs, specifically, causes damage to vascular remodeling, leading to hyperpruned vasculature in the developing retina. Furthermore, we demonstrate that Sema3G maintains vessel stability by enhancing the interaction between β-catenin and VE-cadherin to coordinate barrier maturation in an Nrp2/PlexinD1-dependent manner. We clarify the function of Sema3G in the physiological process of vascular remodeling and the protective role of Sema3G in the treatment of pathological neovascularization. Our study suggests that Sema3G has a beneficial effect on the recovery of ischemic retinopathies.

Results

Sema3G is upregulated in retinas with oxygen-induced retinopathy. Semaphorin signaling is a highly conserved pathway pivotal to vascular patterning (10). To evaluate the distinct role of secreted Sema3s in ischemic retinopathy, we first evaluated the mRNA levels of all members of the Sema3s family in the retinas of oxygen-induced retinopathy (OIR) mouse model (Figure 1A), a well-characterized model that mimics the human pathological process of PDR and ROP (19). In the OIR model, at postnatal day 7 (P7), newborn mice were raised with 75% oxygen until P12. The OIR retinas showed obvious blood vessel loss accompanied by a zone of vaso-obliteration in the center of the retina. When returned to normoxia, these mice developed extraretinal neovascularization during P12 to P17. Subsequently, vessels regrew to the avascular retina, and the preretinal neovascularization regressed during P17 to P25 (19) (Figure 1A). Real-time quantitative PCR (RT-qPCR) revealed a significant increase in *Sema3G* mRNA levels at P17 in OIR retinas compared with retinas from normoxic mice (Figure 1B). As in previous studies (20–22), the mRNA levels of *Sema3A* were upregulated, whereas *Sema3E* was reduced. Interestingly, in the neovascularization regression phase of OIR, we found that the mRNA expression of *Sema3G* was steadily elevated at P19 in OIR retinas compared with retinas from normoxic mice. However, no significant difference in the mRNA levels of other *Sema3s* was detected at P19 (Figure 1B). Furthermore, the phylogenetic relationships of Sema3s revealed evolutionary differences between Sema3G and other Sema3s (Figure 1C), indicating that their pri-

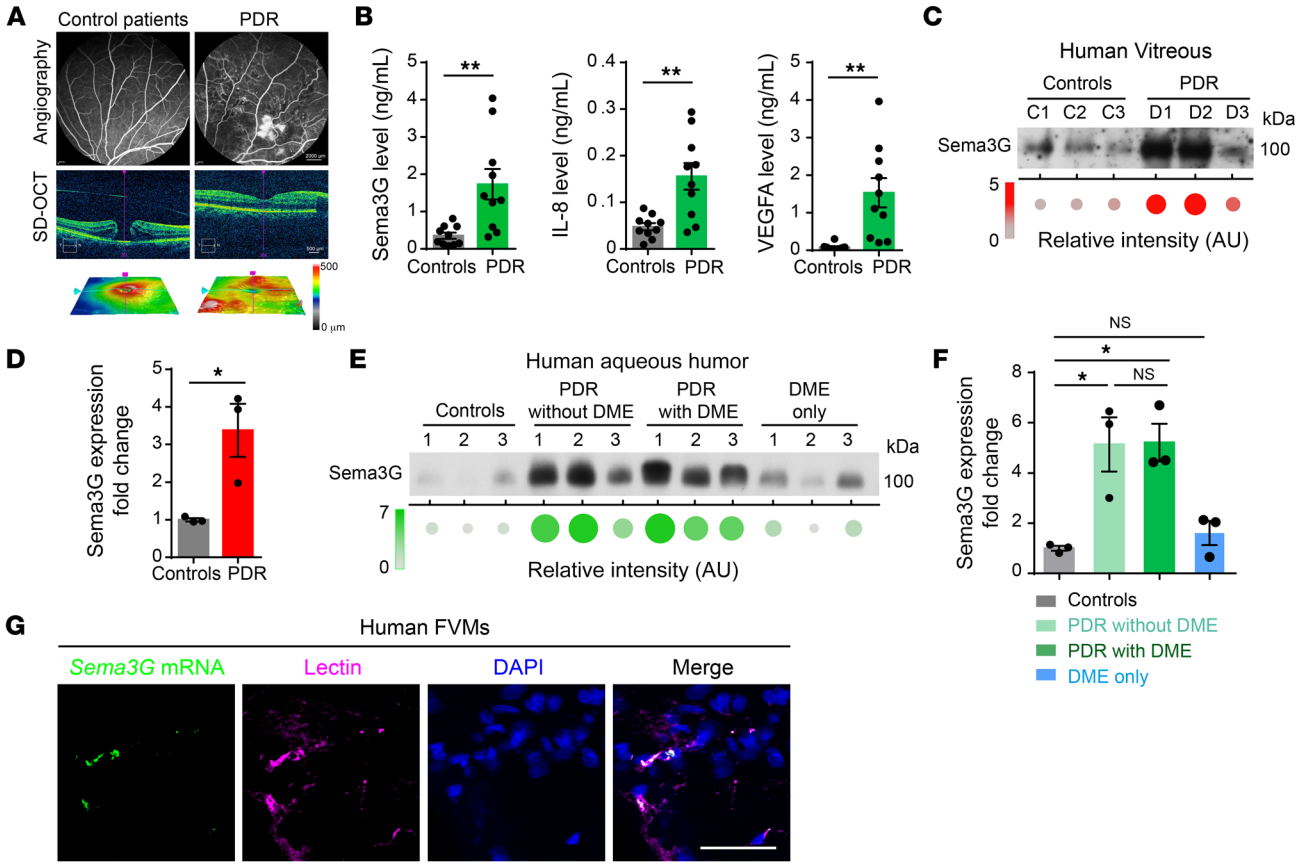

Figure 2. Sema3G is elevated in the vitreous of patients suffering from PDR. (**A**) Angiography and SD-OCT were obtained from patients. Nonvascular ocular pathologies patients served as controls. Scale bars: 2000 μm (top), 500 μm (center). (**B**) ELISA assessment of vitreous fluid shows induction in Sema3G, IL-8, and VEGFA. The results are expressed as the absolute concentrations compared with control patients (n = 10 samples). (**C** and **D**) Immunoblot analysis and quantification of Sema3G protein levels in equal volumes of vitreous fluid from patients (n = 3 samples for each group). (**E** and **F**) Immunoblot analysis and quantification of Sema3G protein levels in equal volumes of aqueous humor from patients with PDR without DME, PDR with DME, and DME only (n = 3 samples for each group). Nondiabetic patients undergoing cataract surgery served as controls. (**G**) RNA in situ hybridization for *Sema3G* mRNA and immunofluorescence for lectin (an EC marker) in fibrovascular membranes (FVMs) of patients suffering from PDR. Error bars represent mean ± SEM, $*P < 0.05$; $**P < 0.01$; 2-tailed Student's t tests (**B** and **D**), 1-way ANOVA with Tukey's multiple comparisons test (**F**). Scale bar: 50 μm (**G**).

mary and spatial structures were different and that Sema3G might perform a different set of functions. Notably, previous studies and RNA-seq data sets have shown that Sema3G was prominently expressed in the vasculature (11, 12, 23), suggesting that the distinctive role of this protein might include essential functions in biological processes related to angiogenesis.

We next examined the mRNA profile of *Sema3G* in the retinas of mice undergoing OIR. mRNA expression analysis revealed no significant difference in *Sema3G* mRNA at P13, whereas it steadily increased from P17 to P25 in OIR retinas compared with retinas from normoxic mice (Figure 1D), indicating that the expression of *Sema3G* continuously increased during the neovascularization regression stage of OIR. However, *Vegfa* mRNA, on the other hand, was mainly increased in the neovascularization phase (Figure 1D). To confirm the elevation of *Sema3G* mRNA in the retina, we assessed the expression of *Sema3G* in the whole-mount retina from OIR and normoxic mice by in situ hybridization. We found that the expression of *Sema3G* mRNA at P19 was significantly upregulated in vessels adjacent to pathological tufts and inside neovascular tufts after OIR, and this expression was restricted to the vessels themselves, as indicated by its colocalization with isolectin B4 (IB4) (Figure 1, E and F). Collectively, these findings suggest an association between the dynamic expression of *Sema3G* and the pathological process of proliferative retinopathies, especially in the phase of neovascularization regression.

Sema3G is elevated in the vitreous fluid of patients with proliferative diabetic retinopathy. Sema3G appears to be a primary vascular-acting semaphorin (11, 17) and is therefore a potential target of interest in manipulating angiogenesis and neovascularization. To assess the potential role of Sema3G in clinical ischemic retinopathy, we investigated the protein levels of Sema3G in the vitreous fluid of patients with PDR. The severity of retinal damage was evaluated by angiography and spectral-domain optical coherence tomography (SD-OCT) (Figure 2A). Patients without vascular pathologies were included as controls (Supplemental Table 1; supplemental material available online with this article; https://doi.org/10.1172/JCI135296DS1). ELISA analysis revealed that the concentration of Sema3G in the vitreous fluid of patients with PDR was significantly higher than that of the controls (Figure 2B). The protein levels of IL-8 and VEGFA, which are representative proin-

flammatory and proangiogenic factors (24, 25), were also elevated in the PDR group (Figure 2B). Western blot analysis further confirmed that Sema3G was elevated in the vitreous fluid of patients with PDR (Figure 2, C and D). We also collected aqueous humor from patients with PDR who did not have diabetic macular edema (DME), patients with PDR with DME, and patients with DME only. The nondiabetic patients who had undergone cataract surgery served as controls (Supplemental Table 2). We found that the protein levels of Sema3G were significantly increased in the group of patients with PDR but not DME as well as in patients with PDR accompanied by DME (Figure 2, E and F). However, the DME-only group did not exhibit higher levels of Sema3G than the control group, indicating that Sema3G might be particularly associated with the pathological process of PDR. In addition, one typical pathological characteristic of PDR is the formation of fibrovascular membranes (FVMs), which are composed of multiple cell types such as glial cells and vascular ECs (26–28). RNA in situ hybridization showed that abundant *Sema3G* mRNA was present and overlapped with lectin in FVMs from patients with PDR (Figure 2G). These results demonstrated that the increased levels of Sema3G protein in the eyes of patients might be derived mainly from the vasculature. Overall, these data provide a rationale for exploring the role of Sema3G in the context of ischemic retinopathy.

Sema3G is expressed exclusively by ECs during retinal angiogenesis. To explore Sema3G spatiotemporal expression in retinal vasculature, the mRNA levels of *Sema3G* were examined in mouse retinas from P2 to P180 (Figure 3A). RT-qPCR analysis revealed that *Sema3G* expression gradually increased with the development of the vascular network (Figure 3B), indicating that Sema3G might play an essential role during retinal development. We also found that *Sema3G* mRNA was markedly expressed in the superficial, intermediate, and deep vascular plexuses of the retina in mice from P6 to P20, as assessed by RNA in situ hybridization (Figure 3C, white arrowheads). *Sema3G* mRNA was specifically colocalized with *CD31* mRNA and lectin staining in retinal sections (Figure 3, D and E, white arrowheads). In agreement with these findings, endogenous Sema3G expression was verified in several representative vascular EC lines (Figure 3F). Furthermore, whole-mount in situ hybridization showed that *Sema3G* mRNA was expressed in both large blood vessels and microvessels (indicated by IB4) in the retina (Figure 3, G and H), but this colocalization was not evident in microglia or astrocytes (Figure 3I). Our results further suggest that *Sema3G* mRNA is present exclusively in retinal ECs during angiogenesis.

Loss of Sema3G leads to decreased vessel density. Sema3G shared a high degree of sequence similarity between primates and several model organisms (Supplemental Figure 1), suggesting that Sema3G was highly evolutionarily conserved and might be an indispensable signaling molecule. To precisely explore the function of Sema3G in angiogenesis under physiological conditions, we bred *Sema3G*$^{fl/fl}$ mice (12) with *Cdh5-Cre* mice, a strain expressing Cre recombinase driven by the Cdh5 promoter (29), and obtained mice with endothelial-specific deletion of *Sema3G* (Supplemental Figure 2A). The reliable reduction in *Sema3G* mRNA levels in *Cdh5-Cre Sema3G*$^{fl/fl}$ mice was detected by RT-qPCR (Supplemental Figure 2B). The high efficiency of Cre-mediated recombination in retinal vessels was also confirmed using an *Ai14* reporter mouse line (Supplemental Figure 2, C and D). Additionally, no significant difference in body weight was found between *Sema3G*$^{fl/fl}$ and *Cdh5-Cre Sema3G*$^{fl/fl}$ mice (Supplemental Table 3).

The retinal vessel forms the superficial vascular plexus at P7. Afterward, the deep and intermediate vascular plexuses develop serially, and 3D vasculature is ultimately formed (Figure 4, A and B) (30, 31). Retinas of *Cdh5-Cre Sema3G*$^{fl/fl}$ mice at P5 and P10 showed decreased vessel density within capillary beds at the retinal leaflet compared with littermate control retinas, as indicated by a decreased percentage of vessel area and increased average vessel length (Figure 4, C and D). However, there was no obvious impairment in radial vessel outgrowth or endothelial sprouting in those retinas (Supplemental Figure 3). In addition, *Cdh5-Cre Sema3G*$^{fl/fl}$ mice had lower vessel density in the deep layer of the retina than their littermates at P14, when retinal vascular networks undergo a process of vascular remodeling during postnatal development (1) (Supplemental Figure 4, A and B). Retinas of *Cdh5-Cre Sema3G*$^{fl/fl}$ mice showed no obvious impairment in vascular branching in the retinal plexuses compared with those of *Sema3G*$^{fl/fl}$ littermates at P20. The characteristics of the vascular network at P60 were also similar between 2 groups (Supplemental Figure 4, C–F). Our data demonstrate that *Sema3G* deficiency in retinal ECs results in hyperpruned vasculature and causes a decrease in vessel density during the early postnatal period, indicating that endothelial Sema3G contributes to the coordination of vascular pruning and remodeling in the retina.

Sema3G coordinates vascular remodeling to form a mature vasculature in vivo. Empty extracellular matrix (ECM) sleeves without ECs in the vascular plexus are well-established indicators of vascular pruning and vessel regression (32–34). To further determine whether loss of Sema3G accelerates the process of vascular remodeling, we performed staining for collagen IV (a marker for ECM) at P6. We found increased empty collagen IV sleeves without ECs at the angiogenic front and in the remodeling plexus in retinas from *Cdh5-Cre Sema3G*$^{fl/fl}$ mice compared with *Sema3G*$^{fl/fl}$ mice (Figure 5, A and B). Consistently, deletion of endothelial Sema3G also resulted in significant deposition of laminin, another ECM protein (Supplemental Figure 5). Notably, we further examined the expression and subcellular localization of VE-cadherin protein, a component of endothelial adherens junctions that is essential for vascular stability. We found that the distribution of VE-cadherin was substantially altered in *Cdh5-Cre Sema3G*$^{fl/fl}$ retinal vessels, where its junctional distribution became discontinuous (Figure 5, C and D). In addition, pericytes are required for the maintenance of vascular stability (35). Pericyte recruitment shown by desmin was decreased in the remodeling plexus in *Cdh5-Cre Sema3G*$^{fl/fl}$ mice (Figure 5, C and D). Our results show that Sema3G deficiency accelerates vessel pruning and causes impairment in vascular remodeling.

To measure the blood-retinal barrier (BRB) function for vascular stability, we injected mice with biocytin-TMR at several postnatal days. The biocytin-TMR ordinarily leaks into the retinal parenchyma from the vessels when a functional BRB is disrupted (36–38). At P7, we observed biocytin-TMR leakage in the distal vessels of *Sema3G*$^{fl/fl}$ and *Cdh5-Cre Sema3G*$^{fl/fl}$ retinas (Supplemental Figure 6, A and B), indicating that the immature distal vessels of retina intrinsically existed in the mice at the early developmental time point (39). However, *Cdh5-Cre Sema3G*$^{fl/fl}$ retinas exhibited

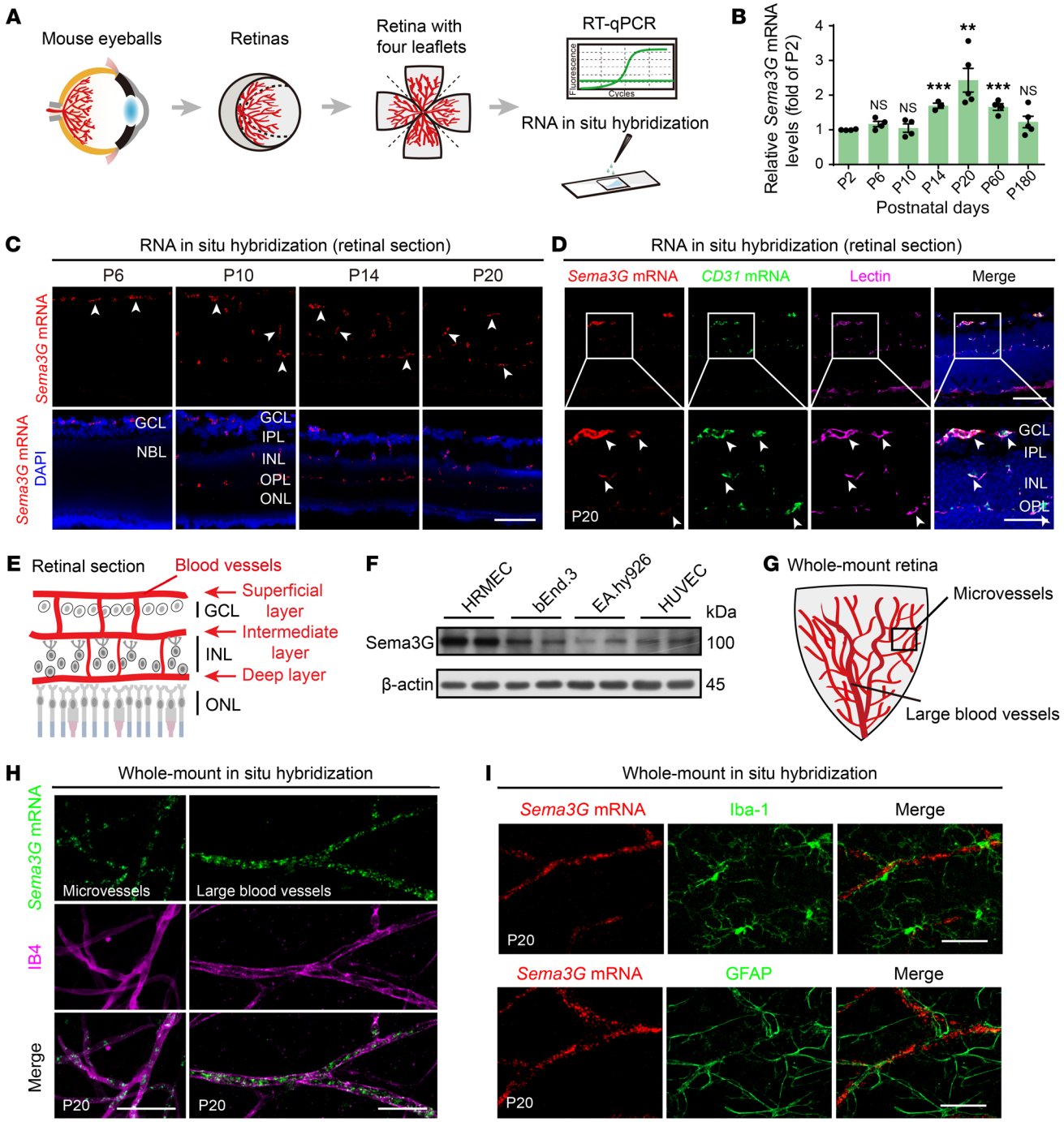

Figure 3. Sema3G is expressed exclusively in ECs in the mouse retina. (**A**) Schematic illustration of retinal preparations for RT-qPCR and RNA in situ hybridization. (**B**) *Sema3G* mRNA expression in the retina at different time points after birth (n = 3–5 mice). (**C**) Representative images of RNA in situ hybridization for *Sema3G* mRNA on retinal sections at P6, P10, P14, and P20 of WT mice. Sema3G is expressed by blood vessels in the superficial, intermediate, and deep layers (white arrowheads). (**D**) Representative images of double fluorescence RNA in situ hybridization for *Sema3G* mRNA (red) and *CD31* mRNA (green) in combination with immunofluorescence for lectin in P20 WT retinas. (**E**) Schematic illustration of the structure of retinal layers and the distribution of vessels in retinal sections. (**F**) Immunoblot analysis of Sema3G protein levels in lysates of primary human retinal microvascular ECs (HRMECs), mouse brain microvascular ECs (bEnd.3 cells), immortalized vascular ECs (EA.hy926), and primary human umbilical vein ECs (HUVECs). (**G**) Schematic illustration of the vascular network in flat-mounted retinas. (**H**) Representative images of RNA in situ hybridization for *Sema3G* mRNA and immunofluorescence for isolectin B4 (IB4) in whole-mounted retinas of WT mice at P20. Sema3G colocalizes with IB4 in microvessels (left panel) and large blood vessels (right panel). (**I**) Representative images of RNA in situ hybridization for *Sema3G* mRNA, in combination with immunofluorescence for Iba-1 (a microglial marker) and GFAP (an astroglial marker) in whole-mount retinas of WT mice at P20. Error bars represent mean ± SEM. $^{**}P < 0.01$; $^{***}P < 0.001$; 2-tailed Student's t tests. Scale bars: 100 μm (**C** and **D**) and 50 μm (**H** and **I**); magnified images: 50 μm (**D**). GCL, ganglion cell layer; NBL, neuroblast layer; IPL, inner plexiform layer; INL, inner nuclear layer; OPL, outer plexiform layer; ONL, outer nuclear layer.

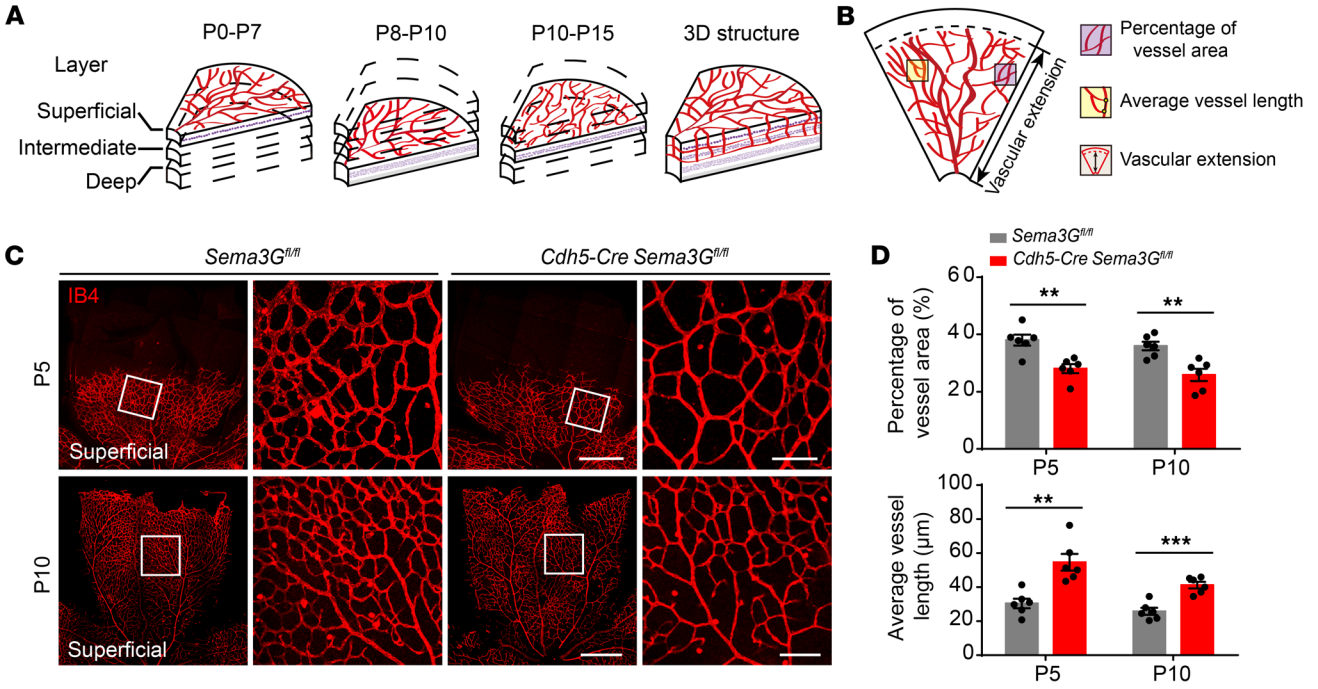

Figure 4. Endothelial Sema3G deletion causes a hyperpruned vascular network in growing retinal vessels. (**A** and **B**) Schematic illustration of the developmental stages during retinal angiogenesis and the quantitative indicators. (**C**) Confocal images showing one-quarter of P5 and P10 flat-mount retinas. Higher magnification images are displayed in the right panel. (**D**) Comparisons of percentage of vessel area and average vessel length of the blood vessels in retinas at P5 or P10 (n = 6 mice for each group). Error bars represent mean ± SEM. $^{**}P < 0.01$; $^{***}P < 0.001$; 2-tailed Student's t tests. Scale bars: 500 μm (**C**); magnified images: 100 μm (**C**).

significant biocytin-TMR leakage at proximal vessels compared with *Sema3G*$^{fl/fl}$ mice, indicating that the hyperpruned vessels in the proximal plexus were immature and more prone to leakage in *Cdh5-Cre Sema3G*$^{fl/fl}$ mice (Supplemental Figure 6, A and B). In addition, conditional EC-specific deletion of *Sema3G* also resulted in higher biocytin-TMR leakage within the retina in the proximal plexus in P10 mice (Supplemental Figure 6, C and D). However, there was no significant biocytin-TMR leakage and no difference in staining of collagen IV or VE-cadherin between P20 *Cdh5-Cre Sema3G*$^{fl/fl}$ and *Sema3G*$^{fl/fl}$ mice (Supplemental Figure 6, C–F).

These data identify that endothelium-derived Sema3G plays an indispensable role in the dynamic process of vascular remodeling at the early developmental stages (Figure 5E), which influences developing vessel pruning, vascular ECM deposition, and the formation of mature vessels.

Endothelial Sema3G deficiency exaggerates neovascularization and vaso-obliteration in OIR retinas. To further explore the role of Sema3G in pathological retinal angiogenesis, we next examined retinas from *Sema3G* knockout mice in different phases of OIR, ranging from P13 to P19. We found that the avascular area and neovascular tuft (NVT) area in *Cdh5-Cre Sema3G*$^{fl/fl}$ mice were quantitatively similar to those in *Sema3G*$^{fl/fl}$ mice in the proliferation phase of OIR, including P13 (Figure 6, A and E) and P15 (Figure 6, B and F). However, *Cdh5-Cre Sema3G*$^{fl/fl}$ mice showed a significantly increased avascular area accompanied by extensive extraretinal NVTs compared with *Sema3G*$^{fl/fl}$ mice at P17 (Figure 6, C and G) and P19 (Figure 6, D and H, and Supplemental Figure 7, A and B) during the stages of pathological vessel regression. These data show that Sema3G simultaneously promotes healthy vascular network formation into the ischemic retina and pathological vessel regression in the diseased vessel remodeling period of OIR.

In addition, vascular leakage and inflammatory cell infiltration are the underlying causes of the exacerbation of retinal vascular diseases (40). We observed that TER119-positive RBC leakage in the *Cdh5-Cre Sema3G*$^{fl/fl}$ retina was increased compared with *Sema3G*$^{fl/fl}$ retinas at P19 in OIR (Figure 6I, and Supplemental Figure 7C), indicating that the vessels of *Cdh5-Cre Sema3G*$^{fl/fl}$ OIR mice were more immature and prone to leakage. Moreover, abundant F4/80-positive macrophages were also found in the *Cdh5-Cre Sema3G*$^{fl/fl}$ OIR mice (Figure 6J, and Supplemental Figure 7D), further suggesting that Sema3G limits vascular leakage and secondary inflammation in the OIR retina. Thus, our data reveal that endogenous Sema3G is required to prevent the exacerbation of vasculopathy in the OIR retina.

Hypoxia increases Sema3G expression in ECs via HIF-2α. We next investigated the mechanism by which endogenous Sema3G hampers vasculopathy in the OIR retina described above. Local nonperfusion causes retinal hypoxia and the release of growth factors, which promotes vascular pathology in the context of PDR (41). Given the observation that Sema3G expression was increased both in mouse OIR retinas and in the eyes of patients with PDR, it prompted us to test whether hypoxia upregulated the expression of Sema3G in ECs. Notably, RT-qPCR revealed that mRNA levels of *Sema3G* and *Vegfa* were both significantly upregulated in bEnd.3 cells exposed to 1% O_2 (Figure 7, A and B).

Hypoxia inducible factors (HIFs) bind to hypoxia response element (HRE, 5′-G/ACGTG-3′) and mediate the expression of certain genes under hypoxic conditions (42, 43). We found

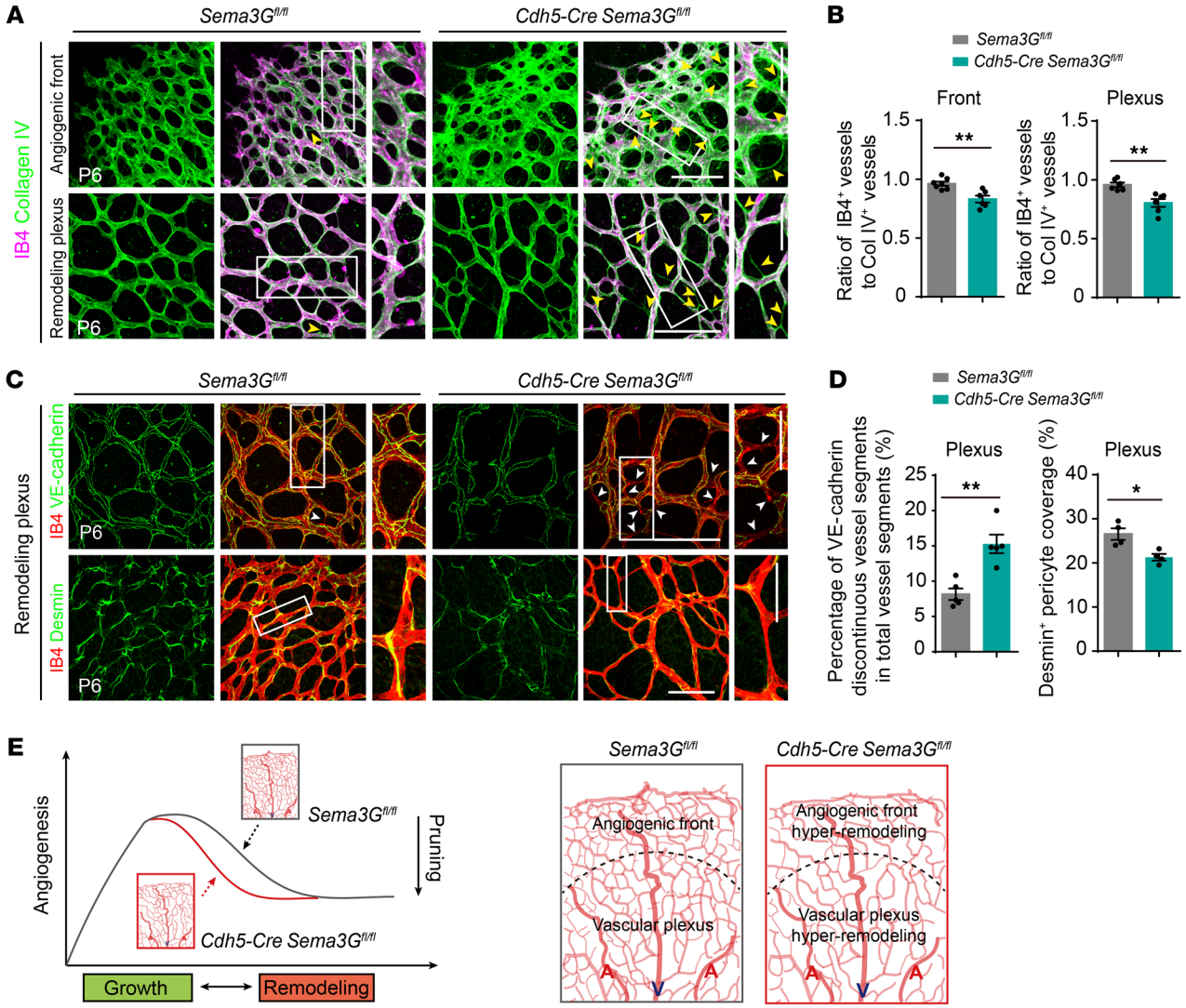

Figure 5. Endothelial Sema3G contributes to the coordination of vascular remodeling. (**A**) Representative images showing increased empty collagen IV–positive (green) but IB4-negative (magenta) matrix sleeves (yellow arrowheads) at the angiogenic front and in remodeling plexus of P6 *Cdh5-Cre Sema3G*$^{fl/fl}$ mice. (**B**) Quantification of the ratio of IB4-positive vessels to collagen IV–positive vessels at the P6 angiogenic front (left, *Sema3G*$^{fl/fl}$, $n = 7$ mice; *Cdh5-Cre Sema3G*$^{fl/fl}$, $n = 6$ mice) and in remodeling plexus (right, $n = 6$ mice for each group). (**C**) Confocal images of anti–VE-cadherin–stained (green) and IB4-stained (red) (upper panel) or anti-desmin–stained (green) and IB4-stained (red) (lower panel) vascular plexus in P6 retinas. Arrowheads indicate EC-EC contacts with absent VE-cadherin signals. (**D**) Quantitation of vessel segments without a continuous junctional VE-cadherin signal (left, normalized to total IB4-labeled segments, $n = 5$ mice) and desmin-positive pericyte coverage in remodeling plexus (right, $n = 4$ mice). (**E**) Schematic illustration of the postnatal retinal angiogenesis model in *Sema3G*$^{fl/fl}$ and *Cdh5-Cre Sema3G*$^{fl/fl}$ mice. The postnatal retinal angiogenesis model could proceed as an overshooting reaction followed by the pruning of excessive vessels. Endothelial Sema3G deletion causes a hyperpruned vascular network in growing retinal vessels. Error bars represent mean ± SEM. $^*P < 0.05$; $^{**}P < 0.01$; 2-tailed Student's *t* tests. Scale bars: 100 μm (**A** and **C**); magnified images: 50 μm (**A** and **C**).

that HIF-1α was elevated rapidly within 1–3 hours after hypoxia, whereas HIF-2α was elevated during the late period of hypoxia (6–24 hours) (Figure 7C, and Supplemental Figure 8, A and B). Interestingly, the time course of Sema3G protein increase was closely correlated with HIF-2α levels (Figure 7C and Supplemental Figure 8C). To investigate the role of HIF-1α and HIF-2α in regulating Sema3G expression, HIF loss-of-function studies were performed using siRNA. RT-qPCR showed that knockdown of HIF-1α had no effects on Sema3G expression under hypoxic conditions (Figure 7D). However, knockdown of HIF-2α significantly downregulated Sema3G expression under hypoxic conditions (Figure 7E). These results were also confirmed by Western blotting (Supplemental Figure 8, D–G). Thus, these data suggest that the expression of endothelial Sema3G is regulated in a HIF-2α–dependent manner upon hypoxia.

We next analyzed the sequence characteristics of the *Sema3G* promoter and identified 3 putative HRE sites (HRE-1, HRE-2, and HRE-3) from the JASPAR database (Figure 7F). To further distinguish the subtype of HIFs that directly binds to the Sema3G promoter and activates its transcription upon hypoxia, a ChIP assay was performed to assess the possibility of HIFs targeting the promoter region of Sema3G. The results showed that the occupancy of HIF-2α, but not HIF-1α, on these HREs was significantly increased upon hypoxic treatments (Figure 7G). We also exam-

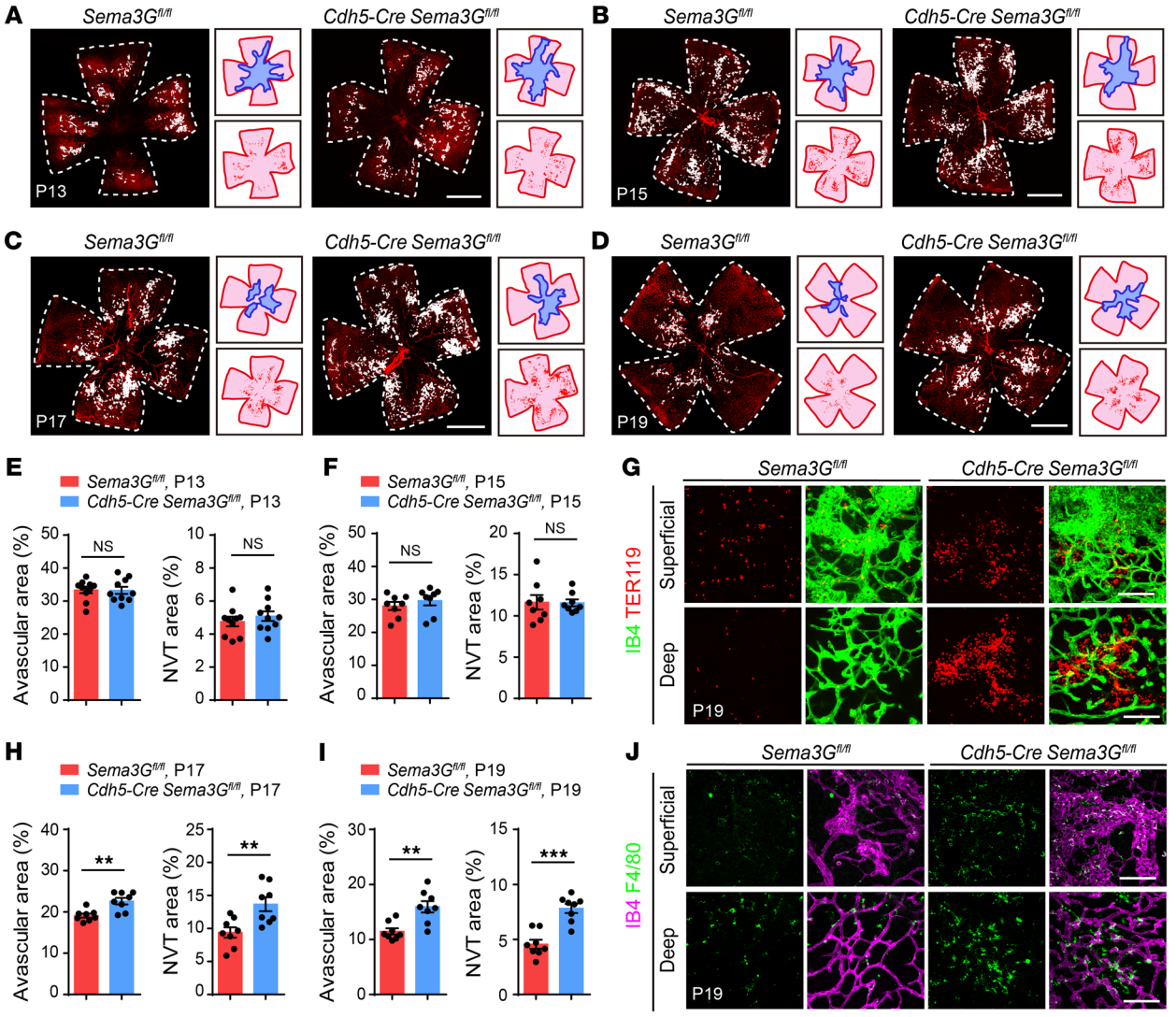

Figure 6. Endothelial Sema3G deficiency significantly delays the regression of pathological vasculature and inhibits vascular normalization in OIR retinas. (**A**–**H**) IB4 staining of whole-mount retinas from *Sema3G*$^{fl/fl}$ and *Cdh5-Cre Sema3G*$^{fl/fl}$ OIR mice at P13 (**A** and **E**, n = 10 mice for each group), P15 (**B** and **F**, n = 8 mice for each group), P17 (**C** and **G**, n = 8 mice for each group), and P19 (**D** and **H**, n = 8 mice for each group) with quantification of the avascular area and neovascular tuft (NVT) area. The white dotted line indicates the edge of the retina, and the white area indicates NVTs. In the insets, the red line indicates the edge of the retina, the blue area indicates the avascular area, and the red area indicates NVTs. (**I** and **J**) TER119-positive RBC leakage and F4/80-positive macrophage infiltration in superficial and deep retinal layers of *Sema3G*$^{fl/fl}$ OIR and *Cdh5-Cre Sema3G*$^{fl/fl}$ OIR mice are shown. Error bars represent mean ± SEM. $^{**}P < 0.01$; $^{***}P < 0.001$; 2-tailed Student's t tests. Scale bars: 1000 μm (**A**–**D**) and 100 μm (**I** and **J**).

ined the ability of these HREs to enhance gene transcription by luciferase reporter assays in HEK293 cells with vectors expressing mutant HREs (Figure 7H). Wild-type HRE significantly increased the luciferase activity in hypoxic cells. Mutation within each HRE site partly abolished hypoxia-induced luciferase activity, whereas increased HRE (5 times HRE) enhanced HRE-driven luciferase activity (Figure 7, H and I). Taken together, these results suggest that HIF-2α directly binds to the Sema3G promoter and activates its transcription upon hypoxia.

Sema3G protects cell-cell junctions by inhibiting β-catenin degradation. To gain better insight into the intracellular molecular mechanisms involved in Sema3G modulating vascular stability, we silenced endogenous Sema3G expression in human retinal microvascular ECs (HRMECs) using a Sema3G-specific short hairpin RNA (shRNA), achieving reduced *Sema3G* mRNA and protein levels (Supplemental Figure 9, A–D). Transcriptome sequencing was carried out to identify the expression profile of control and Sema3G-silenced HRMECs. With an integrated bioinformatics analysis, differentially expressed genes were enriched for Gene Ontology (GO) terms associated with cell adhesion and cell junction (Figure 8A). By Kyoto Encyclopedia of Genes and Genomes (KEGG) pathway analysis, these genes were categorized into cell adhesion molecules, Wnt signaling pathways, and focal adhesions in Sema3G-silenced HRMECs compared with control (Figure 8B). β-Catenin associates with the intracellular segment of VE-cadherin and protects VE-cadherin from degradation, which is required for the regulation of junctional stabilization (44–46), prompting us to examine whether β-catenin plays a crucial role in Sema3G signal-

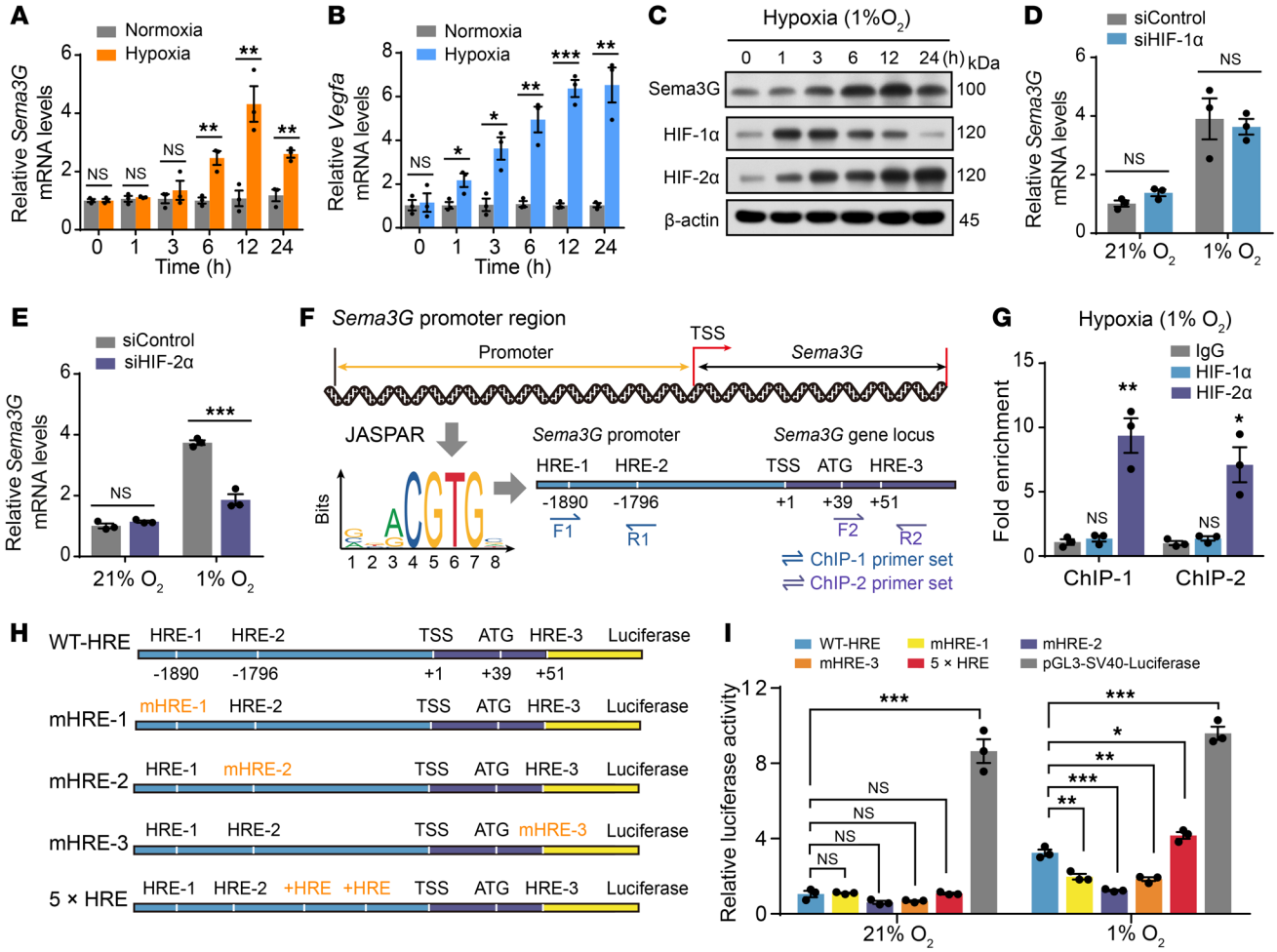

Figure 7. HIF-2α upregulates Sema3G expression upon hypoxia in ECs. (**A** and **B**) *Sema3G* and *Vegfa* mRNA levels in bEnd.3 cells exposed to normoxia (21% O_2) or hypoxia (1% O_2) for the indicated times. Data were normalized to gene expression in cells upon normoxia (n = 3 independent experiments). (**C**) Immunoblot analysis of Sema3G, HIF-1α, and HIF-2α protein in bEnd.3 cells exposed to hypoxia (1% O_2) for the indicated times. (**D** and **E**) RT-qPCR analysis of *Sema3G* mRNA in bEnd.3 cells, which were transfected with siHIF-1α (**D**), siHIF-2α (**E**), or siControl for 48 hours and then exposed to hypoxia (1% O_2) or normoxia (21% O_2) for an additional 12 hours (n = 3 independent experiments). (**F**) Schematic diagram depicting the mouse *Sema3G* promoter with the presence of hypoxia response element (HRE) sequences. HRE sequences from the JASPAR database. ChIP-qPCR primers of the indicated HRE regions are shown. (**G**) ChIP-qPCR assays were performed with the antibodies against HIFs or IgG as control in bEnd.3 cells exposed to 1% O_2 for 12 h (n = 3 independent experiments). (**H**) Diagrammatic representation of mutated HRE (mHRE) introduced into the mouse Sema3G promoter to test HREs in regulating Sema3G transcription. (**I**) Luciferase reporter assay for Sema3G promoter activity in HEK293 cells following transfection of different mHRE vectors (n = 3 independent experiments). Error bars represent mean ± SEM. *P < 0.05; **P < 0.01; ***P < 0.001; 2-tailed Student's t tests (**A**, **B**, **D**, **E**, **G**), 1-way ANOVA with Dunnett's multiple comparisons test (**I**). TSS, transcription start site.

ing. We further knocked out *Sema3G* in HRMECs using CRISPR/Cas9 (Figure 8C and Supplemental Figure 9, E–G) and used antibody staining to test the expression of β-catenin at cell junctions. Consistent with this notion, we observed significantly reduced β-catenin immunostaining at junctions of Sema3G-depleted (also termed Sema3G knockout or Sema3G KO) HRMECs, accompanied by degradation of VE-cadherin (Figure 8D). Next, overexpression of β-catenin rescued junctional β-catenin pools and VE-cadherin stabilization in Sema3G-depleted ECs (Figure 8, D and E).

The levels of β-catenin at the adherens junctions of a cell are regulated by controlling its degradation. Phosphorylation of specific residues of β-catenin leads to its ubiquitination and further degradation (47, 48). To confirm the effect of Sema3G depletion on stability of β-catenin protein, we detected the protein levels of active β-catenin (Ser37 and Thr41 dephosphorylated), phosphorylated β-catenin (p-β-catenin, Ser33/Ser37/Thr41), and total β-catenin in Sema3G-depleted HRMECs. We found that depletion of Sema3G in HRMECs significantly reduced the protein levels of active β-catenin and VE-cadherin. Meanwhile, the levels of phosphorylated β-catenin were upregulated in Sema3G-depleted cells (Figure 8, F–J). Moreover, overexpression of β-catenin reversed the effects of Sema3G depletion on β-catenin and VE-cadherin expression in ECs (Figure 8, F–J). These results together suggest that Sema3G may protect the stabilization of β-catenin from degradation and thus sustain cadherin-mediated adhesion in ECs.

Previous studies demonstrated the essential role of endothelial β-catenin in maintaining barrier integrity (49, 50). We also measured the levels of tight junction proteins in HRMECs via immuno-

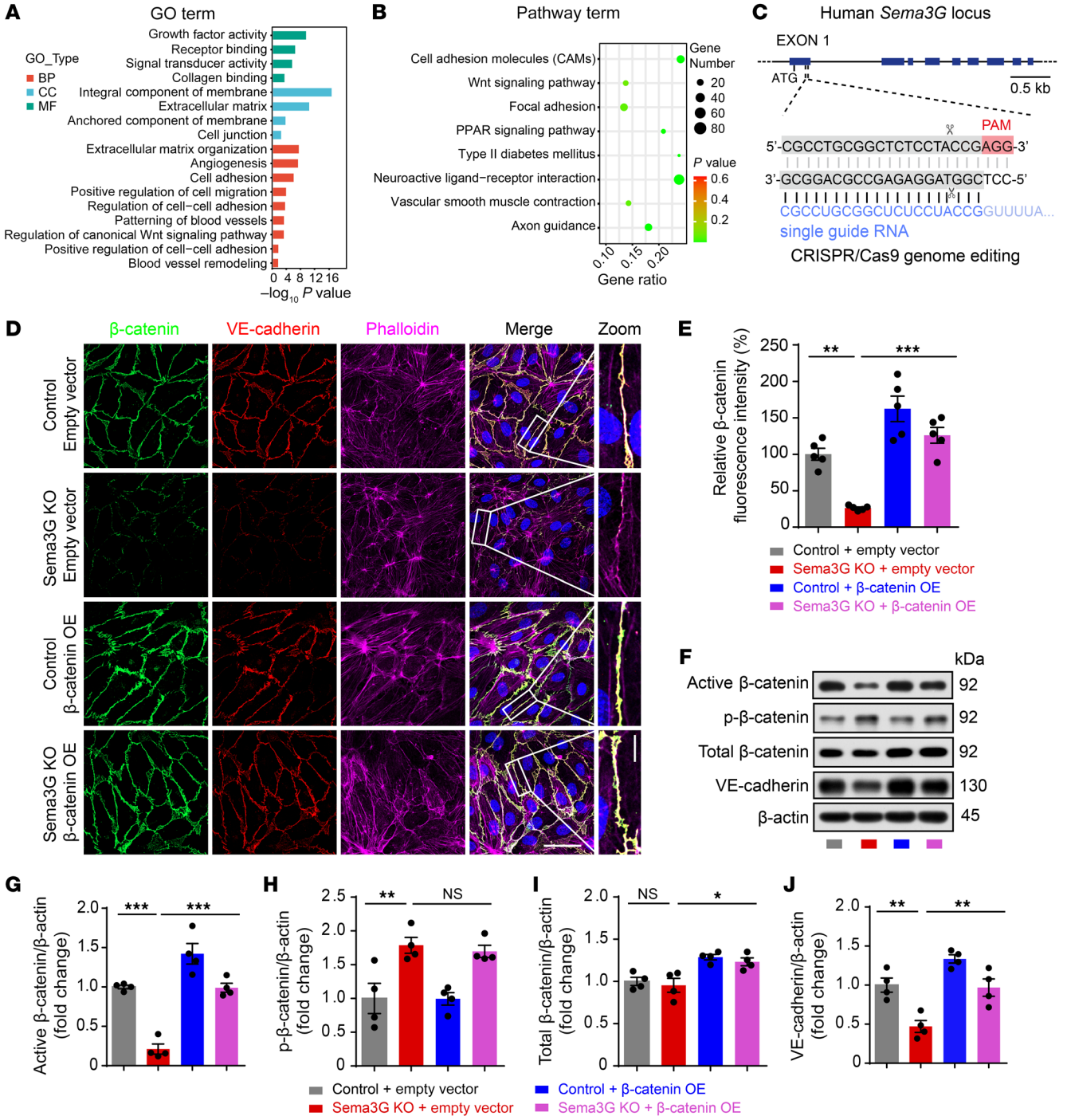

Figure 8. Sema3G deficiency increases the instability of β-catenin. (**A** and **B**) GO terms and KEGG pathway analysis of the differentially expressed genes between control and Sema3G-silenced HRMECs. (**C**) Schematic of the Cas9-sgRNA–targeting sites in the human Sema3G gene. The gray shaded region labels the sgRNA-targeting sequences. (**D**) β-catenin (green), VE-cadherin (red), phalloidin (magenta), and DAPI (blue) staining of control and Sema3G knockout (Sema3G-KO) HRMECs with or without lentivirus-mediated β-catenin overexpression (β-catenin OE). (**E**) Fluorescence signal intensities of β-catenin staining quantified from **D** (n = 5 independent experiments). (**F**–**J**) Immunoblot analysis and quantification of β-catenin and VE-cadherin protein levels in control and Sema3G-KO HRMECs with or without lentivirus-mediated β-catenin OE (n = 4 independent experiments). Error bars represent mean ± SEM. *P < 0.05; **P < 0.01; ***P < 0.001; 1-way ANOVA with Tukey's multiple comparisons test. Scale bars: 50 μm (**D**); magnified images: 10 μm (**D**). PAM, protospacer adjacent motif; p-β-catenin, phosphorylated β-catenin.

fluorescence and Western blotting. Immunofluorescence analysis showed that ZO-1 was reduced at cell-cell junctions after transfection with shSema3G, which was consistent with a significant decrease in ZO-1 protein levels in Sema3G knockdown HRMECs compared with control HRMECs (Supplemental Figure 10, A–D). In addition, Sema3G knockdown did not induce cell apoptosis (Supplemental Figure 10, E and F), eliminating the possibility of apoptosis-mediated breakdown of tight junctions. Collectively,

these results suggest that Sema3G is necessary for the stability of cell-cell junctions in HRMECs.

β-Catenin is required for Sema3G to attenuate ischemic retinopathy. To provide further evidence that β-catenin is a downstream regulator of Sema3G in pathological angiogenesis, we characterized the expression pattern of β-catenin and VE-cadherin in endothelial-specific deletion of *Sema3G* mice in the OIR model. Of note, immunostaining analysis indicated that β-catenin was expressed in vessels adjacent to pathological tufts in vascular front (revascularization) and vascular plexus. Here, β-catenin and VE-cadherin immunostaining were significantly decreased in *Cdh5-Cre Sema3G$^{fl/fl}$* retinal ECs compared with littermate controls (Figure 9, A and B). Moreover, HRMECs were exposed to hypoxia (1% O_2), and immunofluorescence analysis showed that β-catenin and VE-cadherin were also reduced at cell-cell junctions in Sema3G-depleted ECs (Figure 9, C and D). Western blot analysis confirmed the relatively reduced protein expression (Figure 9, E and F). These data imply that β-catenin expression is required for Sema3G-mediated pathological vascular remodeling.

Previous studies showed that lithium chloride (LiCl) exerted an inhibitory effect on the degradation of β-catenin by inhibiting GSK3β, thereby activating Wnt signal transduction (51, 52). Here, we administered LiCl intraperitoneally to the OIR mice (Figure 10, A and B) and found that LiCl was able to rescue the level of β-catenin, especially in the vascular front and vascular plexus, in *Cdh5-Cre Sema3G$^{fl/fl}$* ECs (Figure 10, C and D). In line with the above data, LiCl treatment reduced RBC leakage in *Cdh5-Cre Sema3G$^{fl/fl}$* mice (Figure 10, E and F). Together, our findings demonstrate that Sema3G attenuates ischemic retinopathy by preventing β-catenin degradation, targeting the vasculature for vascular normalization.

The Nrp2/PlexinD1 complex is the functional cell-surface receptor of Sema3G. Neuropilins and plexins form complexes and mediate Sema3s downstream signal transduction, which is responsible for vascular development (10). Our initial analysis demonstrated that Sema3G binds Nrp2 with high affinity (12). Phylogenetic analysis revealed the closest sequence homology of Sema3G with Sema3E (Figure 1C). A previous study showed that Sema3E directly binds to PlexinD1, which is prominently expressed in the developing vasculature as a receptor (53). To further validate the receptors of Sema3G in ECs, HRMECs were transfected with siRNA and then incubated with the alkaline phosphatase–tagged (AP-tagged) recombinant protein Sema3G-AP or Sema3F-AP (a positive control that binds Nrp2 with high affinity) (Supplemental Figure 11A) (54). We found that Sema3G-AP directly bound to siControl or siPlexinD1-transfected HRMECs, but the binding signal was decreased in the absence of Nrp2 (Supplemental Figure 11B), indicating that PlexinD1 was not a direct receptor for Sema3G in ECs. However, the Sema3G-AP binding signal was almost abolished in the absence of both PlexinD1 and Nrp2 (Supplemental Figure 11B). The Sema3F-AP binding signal was decreased in the absence of Nrp2 but was not further affected by PlexinD1 silencing (Supplemental Figure 11B). These results were complemented by COS-7 cells transfected with overexpression vectors of receptors. The binding efficiency of Sema3G-AP to COS-7 cells expressing Nrp2 was greatly enhanced by cotransfection with PlexinD1 (Supplemental Figure 11C), indicating that PlexinD1 acted as a coreceptor for Sema3G. In addition, coimmunoprecipitation (co-IP) experiments revealed that Nrp2 and PlexinD1 bound to each other to form a heterologous receptor complex in HRMECs (Figure 11A). Moreover, the binding of Nrp2 and PlexinD1 was enhanced in the presence of recombinant human Sema3G protein (Figure 11A).

To determine the necessity of PlexinD1 for Sema3G to regulate the stabilization of junctions, we next knocked down PlexinD1 expression in Sema3G-depleted HRMECs and performed Sema3G rescue experiments. Notably, the application of recombinant human Sema3G protein (200 ng/mL) restored junctional β-catenin in Sema3G-depleted HRMECs (Figure 11, B and C). However, the pharmacological effects of Sema3G were abolished when PlexinD1 was knocked down (Figure 11, B and C). This was confirmed using Western blot experiments (Figure 11, D–H). Together, these results provide evidence that Sema3G modulates β-catenin stability in an Nrp2/PlexinD1-dependent manner.

Sema3G attenuates ischemia-induced pathological neovascularization through PlexinD1. To further elucidate the important link between Sema3G and PlexinD1 in retinal vessels in OIR mice, we developed an adeno-associated virus–mediated (AAV-mediated) receptor knockdown method in vivo. Central nervous system microvasculature EC-targeted AAV-BR1 (55) achieved gene silencing in the vasculature of retinas by shRNA targeting PlexinD1 transcripts. We then retro-orbitally injected AAV-shControl or AAV-shPlexinD1 into mice at P7 and P12, and isolated retinas at P19 to identify the silencing effect (Figure 12, A and B). RNA in situ hybridization and Western blot results revealed efficient silencing of PlexinD1 in ECs (Figure 12, C and D, and Supplemental Figure 11, D and E). In addition, AAV-Cre–injected *Ai14* reporter mice were used to verify the infection efficiency of the virus. Robust tdTomato fluorescence was visualized in the retinal blood vessels of AAV-Cre–injected *Ai14* mice (Supplemental Figure 11F), indicating that this AAV was capable of transducing retinal vascular ECs. After confirming that the PlexinD1 receptor was silenced, we intravitreally injected a single dose of 1 μg recombinant Sema3G protein or IgG at P17 into *Cdh5-Cre Sema3G$^{fl/fl}$* mice that were transfected with AAV-shControl or AAV-shPlexinD1 undergoing OIR and then analyzed the retinas at P19 (Figure 12B). Treatment of *Cdh5-Cre Sema3G$^{fl/fl}$* mice with recombinant Sema3G significantly suppressed NVT formation and decreased the avascular area (Figure 12, E–G). However, Sema3G failed to ameliorate pathological neovascularization in *Cdh5-Cre Sema3G$^{fl/fl}$* mice treated with AAV-shPlexinD1 (Figure 12, E–G). These results provide evidence that PlexinD1 is essential for Sema3G signal transduction in the pathological process of retinopathy.

Endothelial Sema3G is required for pathological vessel regression in choroidal neovascularization models. To further explore the potential role of Sema3G in pathological choroidal neovascularization, we next studied retinas from endothelial-specific *Sema3G* knockout mice in a laser-induced choroidal neovascularization (CNV) mouse model (56, 57). After Bruch's membrane is damaged by a laser, new vessels grow from choroidal vessels toward the retina, then CNV begins to spontaneously regress on the seventh day (57–59). Both *Sema3G$^{fl/fl}$* and *Cdh5-Cre Sema3G$^{fl/fl}$* mice were treated with the same laser to induce CNV at P20 or P60, respectively. The leakage and CNV volume were measured by fluorescein angiography (FA) and indocyanine green angiography (ICGA) in vivo on day 14 after laser treatment. Next, the whole-mount choroids were immunostained with IB4 for quantitative analysis of laser-induced neovascular

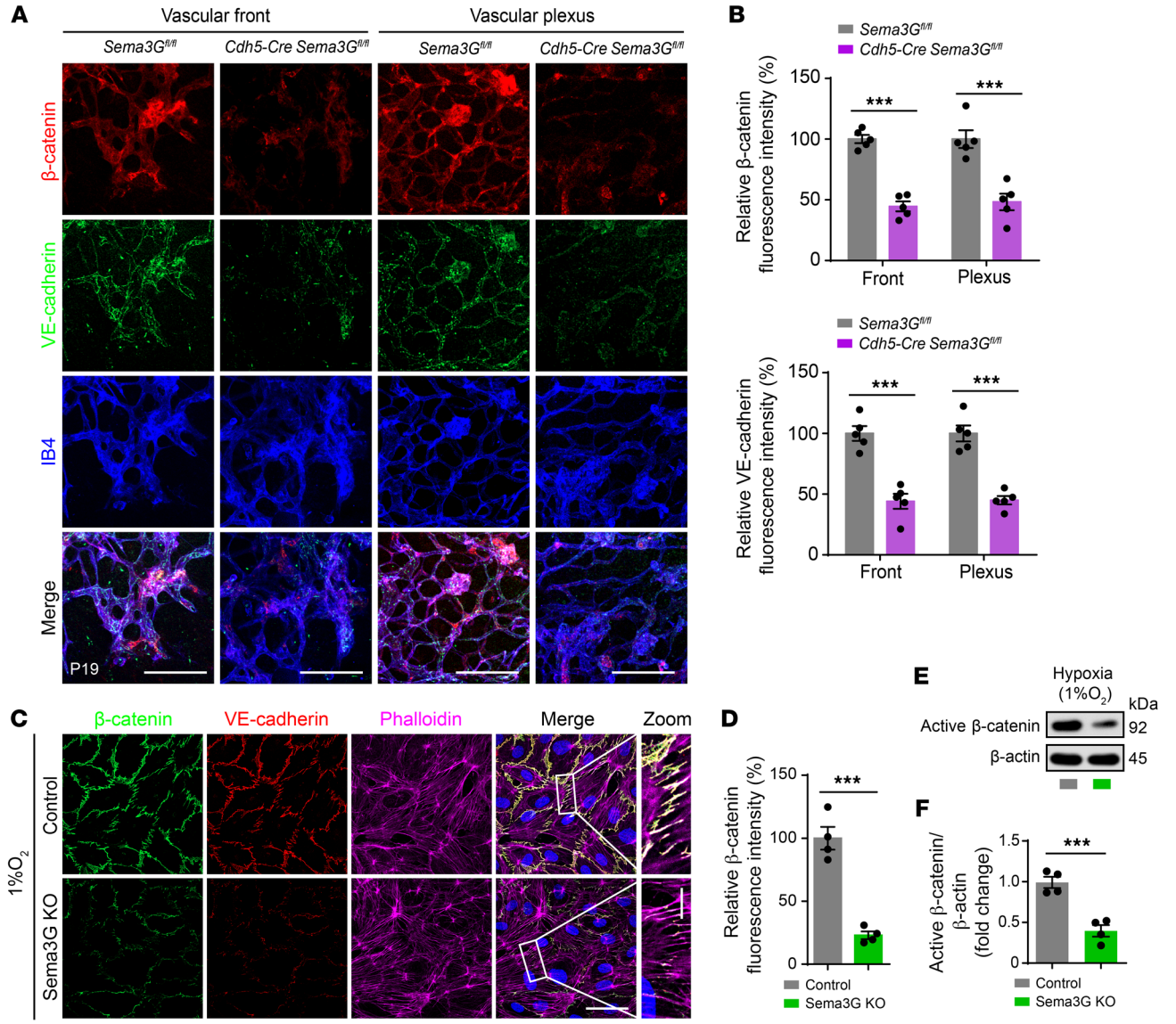

Figure 9. Reduction in the expression of β-catenin as a result of Sema3G deficiency in OIR mice. (**A**) Representative images of β-catenin (red) and VE-cadherin (green) expression in IB4-positive (blue) vessels at the vascular front (revascularization) and vascular plexus in *Sema3G*$^{fl/fl}$ OIR and *Cdh5-Cre Sema3G*$^{fl/fl}$ OIR mice at P19. (**B**) Fluorescence signal intensities of β-catenin and VE-cadherin staining quantified from **A** (n = 5 mice for each group). (**C**) Representative β-catenin staining in control and Sema3G-KO HRMECs following hypoxia (1% O_2) treatment. (**D**) Fluorescence signal intensities of β-catenin staining quantified from **C** (n = 4 independent experiments). (**E** and **F**) Immunoblot analysis and quantification of β-catenin protein levels in control and Sema3G-KO HRMECs following hypoxia (1% O_2) treatment (n = 4 independent experiments). Error bars represent mean ± SEM. ***P < 0.001; 2-tailed Student's t tests. Scale bars: 100 μm (**A**) and 50 μm (**C**); magnified images, 10 μm (**C**).

area (Supplemental Figure 12, A and D). At 14 days after laser photocoagulation, our results showed that *Cdh5-Cre Sema3G*$^{fl/fl}$ mice exhibited markedly increased vascular leakage assessed by FA and enlarged CNV volume labeled with IB4 compared with *Sema3G*$^{fl/fl}$ mice (Supplemental Figure 12, B, C, E, and F). Taken together, these data reveal that endothelium-derived Sema3G is also required for pathological vessel regression in the CNV model.

Sema3G supplementation enhances revascularization of the ischemic retina. To explore the beneficial effects of Sema3G in pathological angiogenesis, we designed an AAV carrying the Sema3G coding sequence and administered it to the developing retina at P7 and P12 (Figure 13, A and B). The expression of Sema3G was significantly increased at P19 after injection of the AAV-Sema3G into mice (Figure 13, C and D). Notably, injection of AAV-Sema3G into *Sema3G*$^{fl/fl}$ mice obviously decreased NVT formation and the average avascular area compared with AAV-Control injected into *Sema3G*$^{fl/fl}$ mice (Figure 13, E–G), while injection of AAV-Sema3G into *Cdh5-Cre Sema3G*$^{fl/fl}$ mice resulted in the restoration of the phenotypes (Figure 13, E–G). These results demonstrate that endothelial Sema3G is indispensable for normal retinal recovery and pathological vessel regression in the ischemic retina.

In addition, to investigate the protective effects of Sema3G, we also performed an in vivo Matrigel plug assay (Supplemental Figure 13, A–E) (32). The presence of basic fibroblast growth fac-

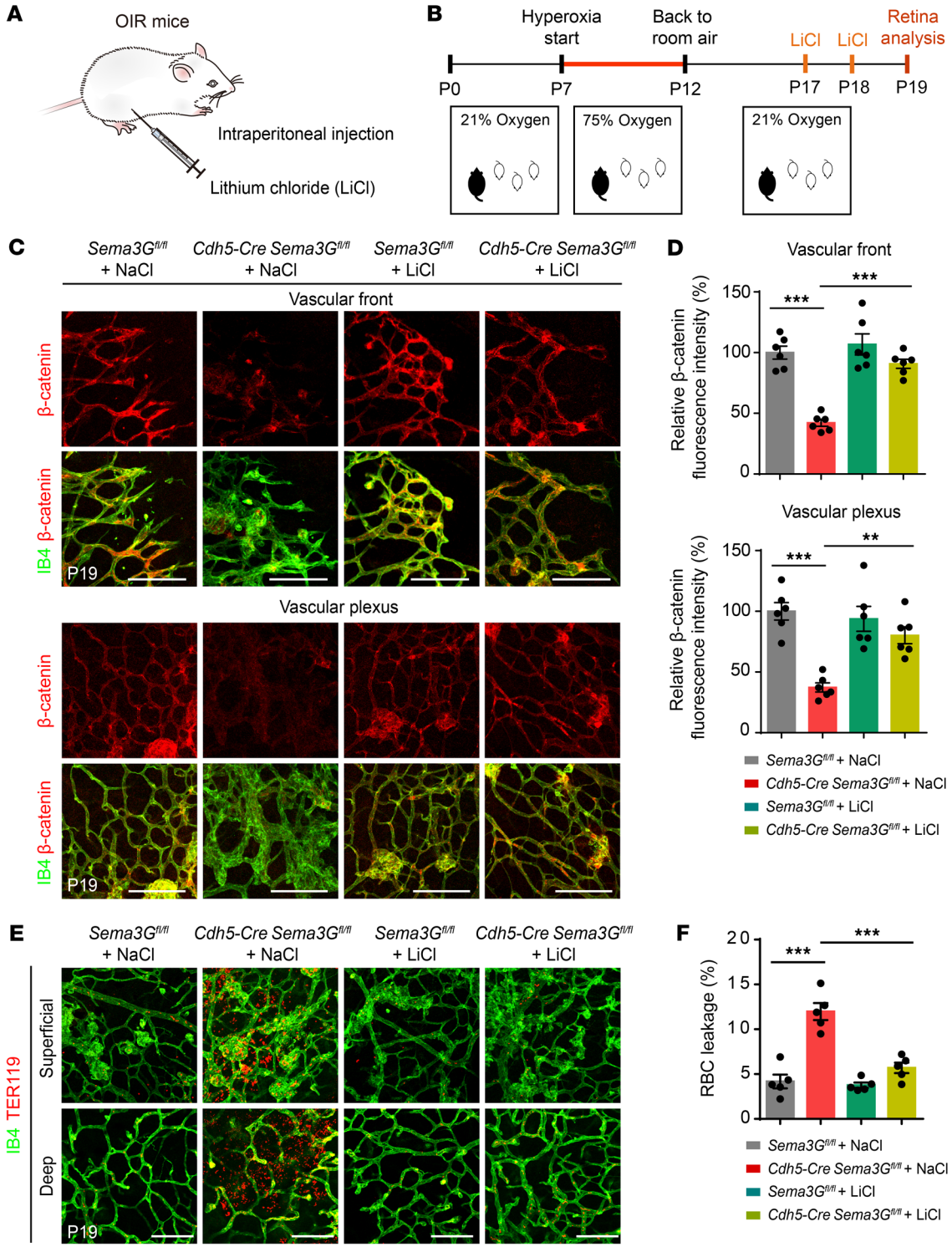

Figure 10. Sema3G regulates vascular regeneration and decreases hemorrhage by stabilizing β-catenin expression in OIR. (**A** and **B**) Lithium chloride (LiCl) or sodium chloride (NaCl, as control) was administered to the OIR mice by intraperitoneal injection. At P17 and P18, OIR mouse pups were intraperitoneally injected with NaCl or LiCl. Then, retinas were analyzed at P19. (**C**) Expression of β-catenin at the vascular front (revascularization) and vascular plexus in IB4-stained P19 retinas of *Sema3G*$^{fl/fl}$ OIR and *Cdh5-Cre Sema3G*$^{fl/fl}$ OIR mice treated with NaCl or LiCl. (**D**) Fluorescence signal intensities of β-catenin staining quantified from **C** (n = 6 mice for each group). (**E**) Representative images showing TER119-positive RBC leakage in superficial and deep retinal layers of *Sema3G*$^{fl/fl}$ OIR and *Cdh5-Cre Sema3G*$^{fl/fl}$ OIR mice treated with NaCl or LiCl. (**F**) Quantification of RBC leakage in *Sema3G*$^{fl/fl}$ OIR and *Cdh5-Cre Sema3G*$^{fl/fl}$ OIR mice as shown in **E** (n = 5 mice for each group). Error bars represent mean ± SEM. $^{**}P < 0.01$; $^{***}P < 0.001$; 1-way ANOVA with Tukey's multiple comparisons test. Scale bars: 100 μm (**C** and **E**).

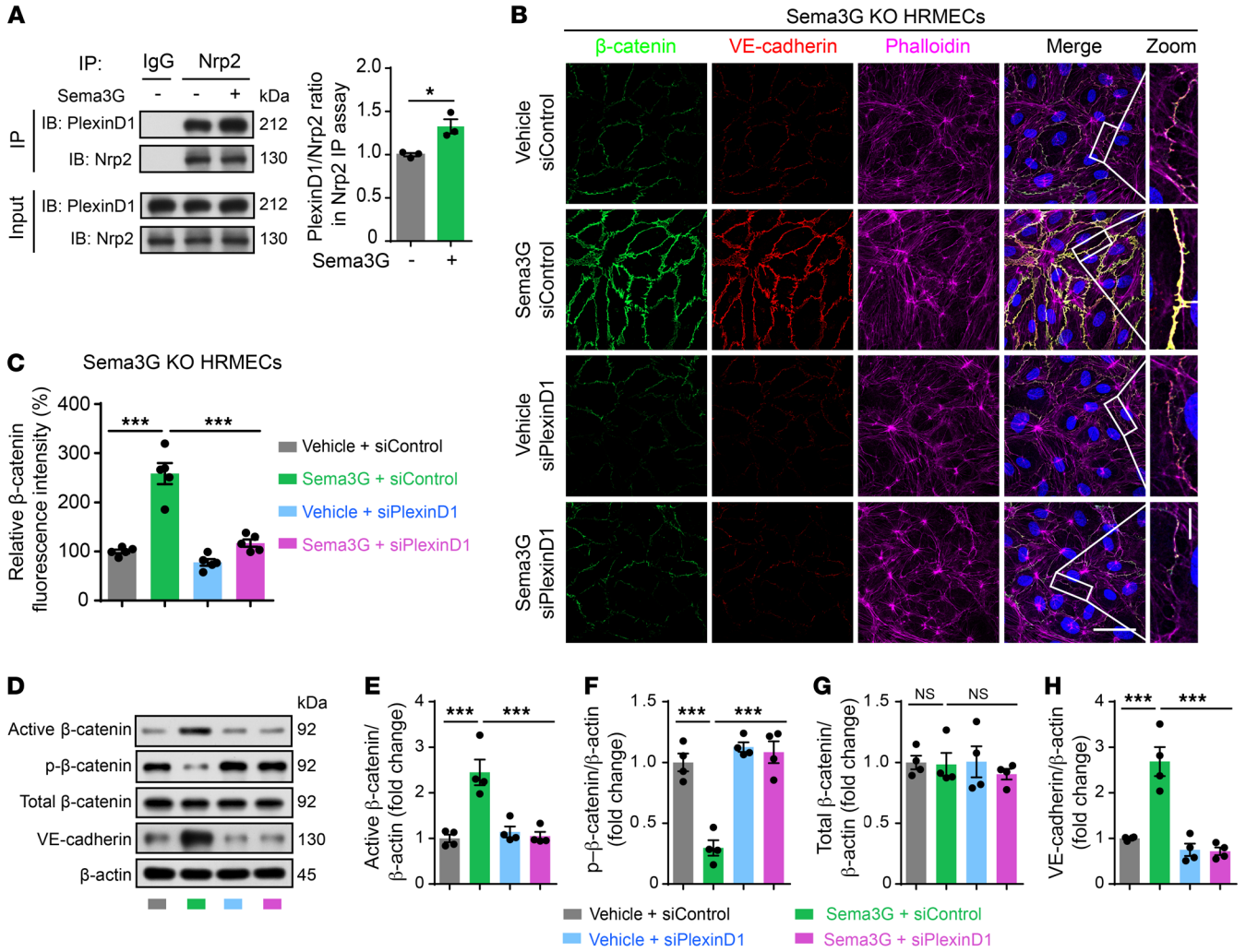

Figure 11. Sema3G modulates β-catenin stability in an Nrp2/PlexinD1-dependent manner. (**A**) Immunoprecipitated (IP) Nrp2 was immunoblotted (IB) with Nrp2 or PlexinD1 antibody in HRMECs (n = 3 independent experiments). (**B**) Representative β-catenin and VE-cadherin staining in Sema3G-KO HRMECs treated with siControl or siPlexinD1 and then incubated with or without recombinant Sema3G protein. (**C**) Fluorescence signal intensities of β-catenin quantified from **B** (n = 5 independent experiments). (**D**–**H**) Immunoblot analysis and quantification of β-catenin and VE-cadherin protein levels in Sema3G-KO HRMECs treated with siControl or siPlexinD1 and then incubated with or without recombinant Sema3G protein (n = 4 independent experiments). Error bars represent mean ± SEM. *P < 0.05; ***P < 0.001; 2-tailed Student's t tests (**A**) and 1-way ANOVA with Tukey's multiple comparisons test (**C**, **E**–**H**). Scale bars: 50 μm (**B**); magnified images: 10 μm (**B**).

tor (bFGF) could induce the formation of a stable vascular network (60); however, the leakage of 10 kDa tetramethylrhodamine (TRITC)–dextran was observed in the $VEGFA_{165}$ group, indicating that $VEGFA_{165}$ induced the formation of highly permeable pathological vessels (Supplemental Figure 13F) (61). Notably, overexpression of Sema3G resulted in a reduction in 10 kDa TRITC-dextran dispersing outside of the vessels in the presence of $VEGFA_{165}$ (Supplemental Figure 13, F and G). These data suggest that Sema3G protects pathological vessels from leakage and controls the stabilization of angiogenesis.

To further determine whether local Sema3G administration provides therapeutic effects following OIR, we intravitreally injected a single dose of 1 μg recombinant Sema3G protein or IgG into *Sema3G*$^{fl/fl}$ or *Cdh5-Cre Sema3G*$^{fl/fl}$ mice undergoing OIR at P15 and analyzed the retinas at P17 (Figure 13, H–J). We found that treatment of *Sema3G*$^{fl/fl}$ mice with recombinant Sema3G significantly suppressed NVT formation and decreased the avascular area compared with IgG treatment (Figure 13, K–M). Moreover, intravitreal injection of recombinant Sema3G into *Cdh5-Cre Sema3G*$^{fl/fl}$ mice also resulted in decreased NVTs and avascular area (Figure 13, K–M). Overall, these data demonstrate the protective effect of Sema3G on ischemia-induced neovascularization and imply that Sema3G supplementation can be established as a promising treatment approach for preventing the exacerbation of vasculopathy in the OIR model.

Discussion

There is an urgent need to improve the current pharmacological treatment modalities for retinal neovascular diseases (3, 4). Retinal hypervascularization is characterized by the failure of vascularization of the retina, leading to compensatory pathological angiogenesis to reinstate metabolic equilibrium (3). The present study provides the first evidence that Sema3G is elevated in the

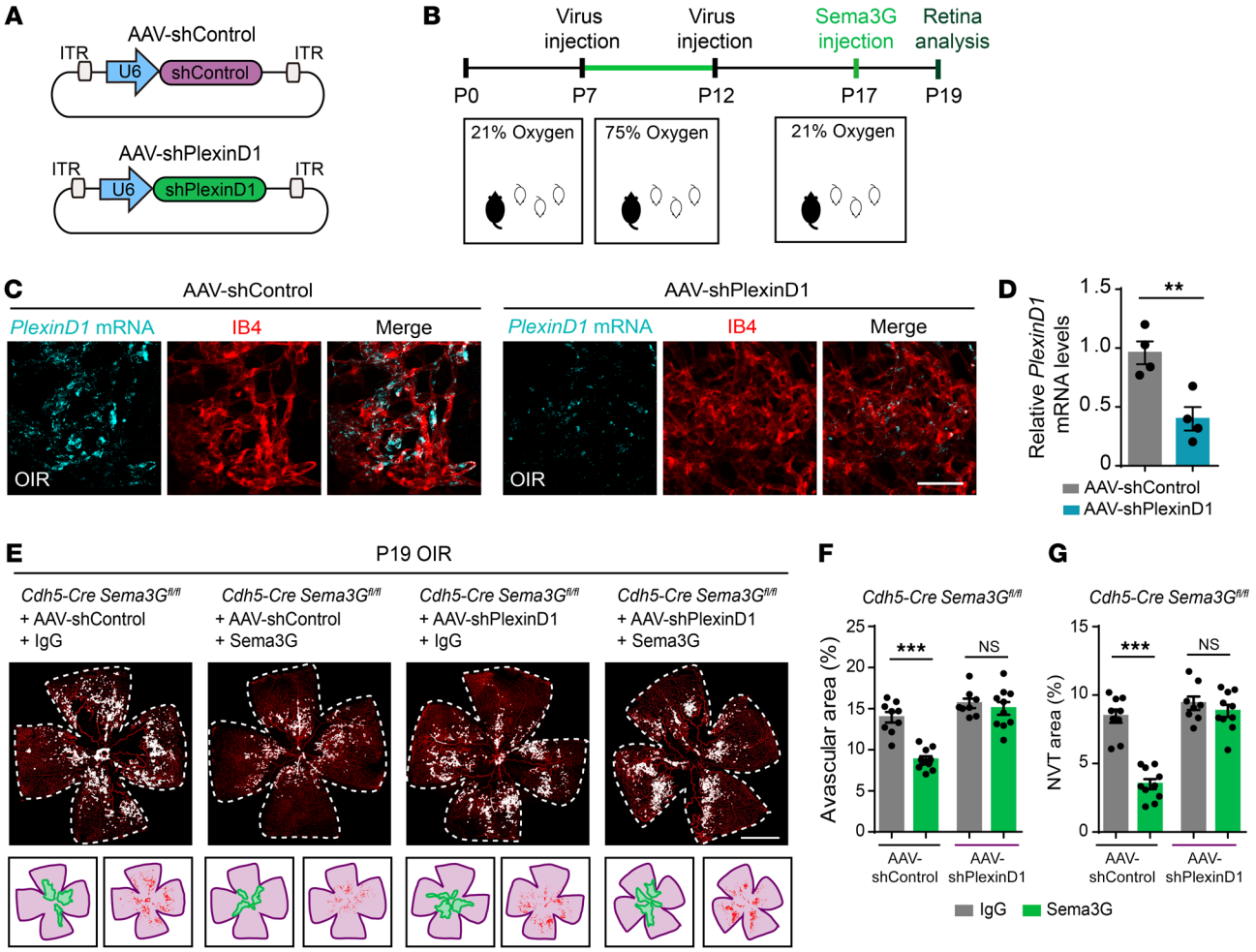

Figure 12. PlexinD1 is necessary for the functional performance of endothelial Sema3G against pathological neovascularization. (**A**) Schematic diagram of the AAV used for PlexinD1 knockdown in vivo. (**B**) Transduction of ECs with AAV in *Cdh5-Cre Sema3G*$^{fl/fl}$ OIR mice. Neonatal mice were injected through the retro-orbital sinus with AAV at P7 and P12. At P17, mouse pups were intravitreally injected with 1 μg IgG or recombinant Sema3G. Retinas were analyzed at P19. (**C**) Representative images of RNA in situ hybridization for *PlexinD1* mRNA in whole-mounted retinas of OIR mice. (**D**) Quantification of *PlexinD1* mRNA in OIR retinas in **C** (n = 4 mice for each group). (**E**) IB4 staining of retinas from *Cdh5-Cre Sema3G*$^{fl/fl}$ OIR mice transduced with AAV-shControl or AAV-shPlexinD1 and treated with or without recombinant Sema3G protein. (**F** and **G**) Quantification of the avascular area and NVT area at P19 in OIR, related to **E** (n = 9, 10, 8, and 10 mice for *Cdh5-Cre Sema3G*$^{fl/fl}$ + AAV-shControl + IgG, *Cdh5-Cre Sema3G*$^{fl/fl}$ + AAV-shControl + Sema3G, *Cdh5-Cre Sema3G*$^{fl/fl}$ + AAV-shPlexinD1+ IgG and *Cdh5-Cre Sema3G*$^{fl/fl}$ + AAV-shPlexinD1 + Sema3G groups, respectively). Error bars represent mean ± SEM. $^{**}P < 0.01$; $^{***}P < 0.001$; 2-tailed Student's t tests (**D**) and 1-way ANOVA with Tukey's multiple comparisons test (**F** and **G**). Scale bars: 50 μm (**C**) and 1000 μm (**E**).

vitreous fluid and aqueous humor of patients with PDR. Endothelial Sema3G deficiency accelerates pathological angiogenesis, whereas Sema3G supplementation prevents excessive pathological angiogenesis in the OIR model. Mechanistically, HIF-2α directly regulates Sema3G expression in ECs under hypoxic pathological processes. Our observations also indicate a specific mode of action by which Sema3G preserves vascular stability by improving endothelial β-catenin and VE-cadherin stabilization via the Nrp2/PlexinD1 signaling pathway (Figure 14).

Notably, in OIR mice, Sema3G expression appears to be enhanced in the neovascularization regression stage, whereas VEGFA expression is increased immediately in the proliferation stage after vessel loss. These findings are consistent with the functional roles of VEGFA in mediating retinal angiogenesis and vascular leakage during hypoxic conditions (62). Here, we report an interesting finding that loss of Sema3G in retinal vascular ECs causes markedly increased retinal vaso-obliteration, neovascularization, and vascular leakage, which are features of neovascular retinopathy, at stages of diseased blood vessel remodeling and regression in retinopathy. Therefore, it can be assumed that Sema3G is a critical factor that protects against the existence of pathological vessels. Previously, it has also been reported that Sema3G possesses antiangiogenic and antitumorigenic properties, which results in a decrease in tumor-associated vessel density (14–16). The antitumorigenic activity of class 3 semaphorins can be explained by competition with VEGF for Nrp binding (14). These prior findings support our conclusion that Sema3G may be a potential therapeutic target for certain hypervascularization diseases.

Notably, we found that intravitreal injection of recombinant Sema3G proteins effectively reduces pathological angiogenesis and guides the formation of a stable vascular network during the neovascularization regression stage. Intravitreal therapy with neu-

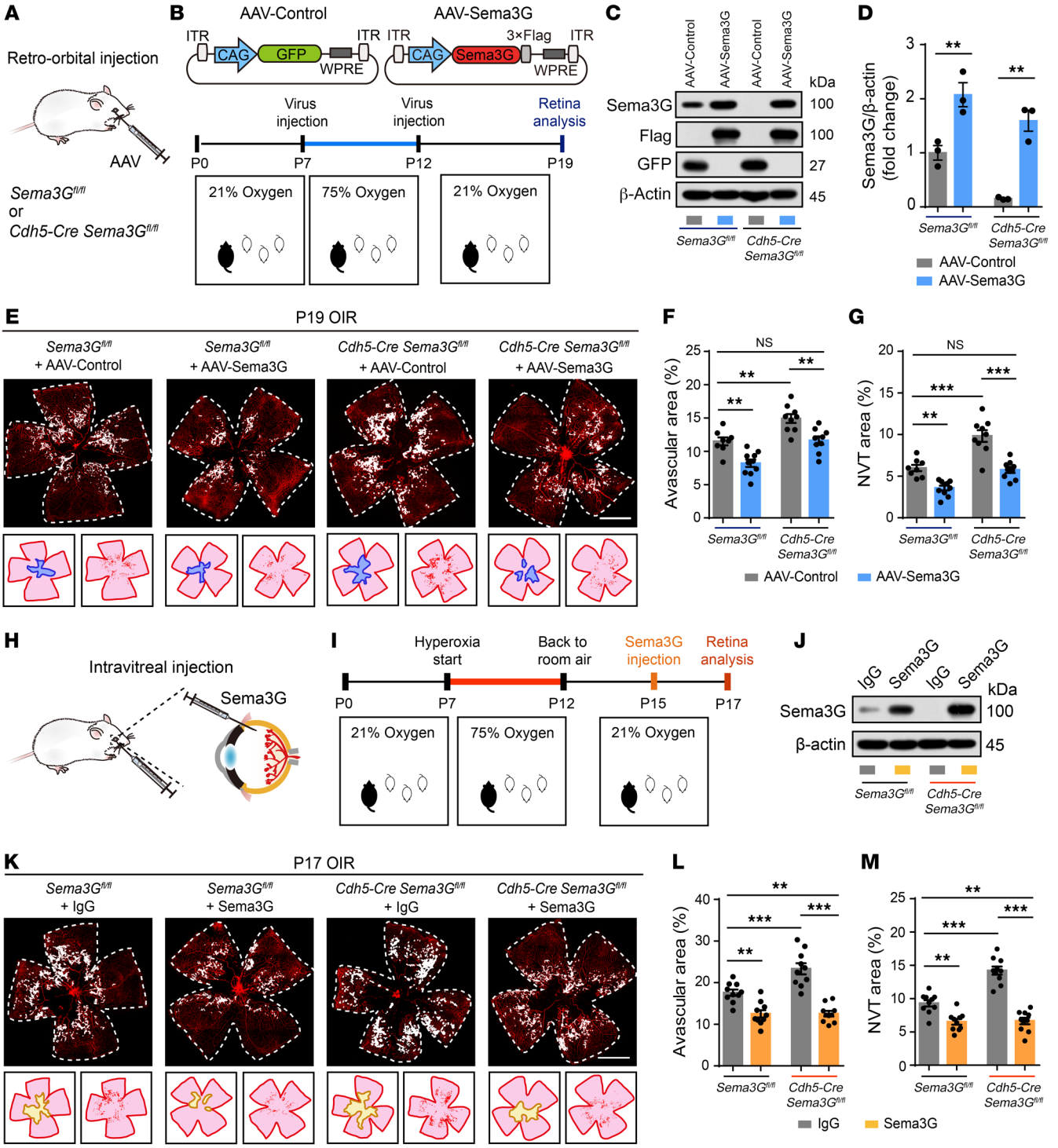

Figure 13. Supplementation of Sema3G ameliorates ischemic retinopathy in the OIR model. (**A** and **B**) Transduction of ECs with AAV in *Sema3G*$^{fl/fl}$ and *Cdh5-Cre Sema3G*$^{fl/fl}$ OIR mice. Neonatal mice were injected through the retro-orbital sinus with AAV-Control or AAV-Sema3G at P7 and P12. The retinas were analyzed at P19. (**C** and **D**) Immunoblots and quantification analysis showed overexpression of Sema3G in the retinas of AAV-Sema3G–injected mice compared with AAV-Control–injected mice (n = 3 independent experiments). (**E**) IB4 staining of whole-mount retinas from OIR mice infected with AAV-Control or AAV-Sema3G. (**F** and **G**) Quantification of the avascular areas and the NVT area at P19 in OIR, related to **E** (n = 8, 10, 9, and 9 mice for *Sema3G*$^{fl/fl}$ + AAV-Control, *Sema3G*$^{fl/fl}$ + AAV-Sema3G, *Cdh5-Cre Sema3G*$^{fl/fl}$ + AAV-Control and *Cdh5-Cre Sema3G*$^{fl/fl}$ + AAV-Sema3G groups, respectively). (**H** and **I**) Schematic illustration of the OIR mice treated with intravitreal injections of recombinant Sema3G. At P15, mouse pups were intravitreally injected with 1 μg IgG or recombinant Sema3G. Retinas were analyzed at P17. (**J**) Entire eye samples of mice were harvested and homogenized, then prepared for immunoblot analysis of total Sema3G protein abundance. (**K**) IB4 staining of whole-mount retinas from *Sema3G*$^{fl/fl}$ and *Cdh5-Cre Sema3G*$^{fl/fl}$ OIR mice injected with IgG or recombinant Sema3G. (**L** and **M**) Quantification of the avascular area and NVT area at P17 in OIR, related to **K** (n = 10, 10, 10, and 10 mice for *Sema3G*$^{fl/fl}$ + IgG, *Sema3G*$^{fl/fl}$ + Sema3G, *Cdh5-Cre Sema3G*$^{fl/fl}$ + IgG and *Cdh5-Cre Sema3G*$^{fl/fl}$ + Sema3G groups, respectively). Error bars represent mean ± SEM. $^{**}P < 0.01$; $^{***}P < 0.001$; 1-way ANOVA with Tukey's multiple comparisons test. Scale bars: 1000 μm (**E** and **K**).

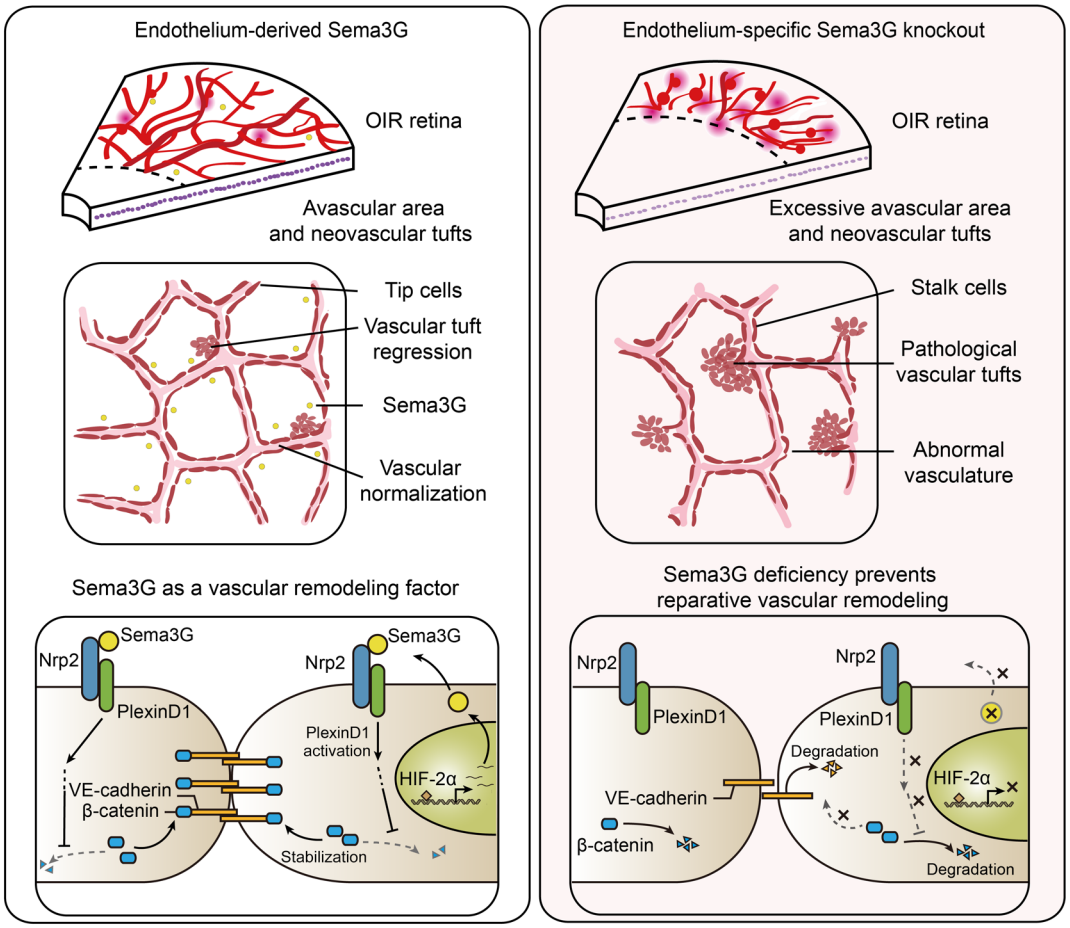

Figure 14. Schematic illustration of the mechanism by which endothelium-derived Sema3G attenuates ischemic retinopathy. Loss of *Sema3G* in endothelial cells aggravated pathological angiogenesis in OIR mice. Sema3G functions as an essential defense mechanism deployed by the vasculature to promote pathological blood vessel regression and to promote vascular normalization during vessel remodeling. Mechanistically, we demonstrated that HIF-2α directly regulated *Sema3G* transcription in ECs under hypoxia. Sema3G coordinated the functional interaction between β-catenin and VE-cadherin by increasing β-catenin stability in the endothelium through the Nrp2/PlexinD1 receptor. Furthermore, Sema3G supplementation enhanced healthy vascular network formation and promoted diseased vasculature regression.

tralizing VEGF antibodies has been an important treatment for these retinal vascular diseases in the clinic (5, 6). However, some patients with vascular diseases are refractory to anti-VEGF therapy (7). Based on our results, we speculate that Sema3G is an important vascular protective factor. Future studies should continue to focus on uncovering the therapeutic effects of Sema3G on the OIR mouse model and further explore whether recombinant Sema3G proteins can be considered in combination with anti-VEGF neutralizing antibodies to treat neovascular diseases owing to the beneficial impact of Sema3G on regression of pathological blood vessels. In addition, our results highlight that AAV-mediated endothelial Sema3G overexpression seems to exert sufficient therapeutic effects and offers the potential for long-lasting gene therapy, which solves several therapeutic challenges, including the need for frequent intravitreal injections and the risk of patient compliance affecting therapeutic outcomes. These insights provide rational drug targets to intervene with pathological angiogenesis and regression.

Interestingly, we found that the presence of HIF-2α regulates Sema3G expression, which can explain why the Sema3G level is increased in the later phase of hypoxia. Proliferative retinopathies are characterized by ischemia-induced neovascularization regulated by HIF pathways (41). HIFs play a central role in regulating a host of proangiogenic genes, such as those involved in vascular permeability, angiogenesis, and oxygen homeostasis (42). A previous study showed that HIF-1α mainly stimulated the expression of alcohol metabolic, hexose metabolic, and glycolytic genes, whereas HIF-2α induced the expression of developmental genes such as angiopoietin 2 (Angpt2) and Fms-like tyrosine kinase 1 (Flt-1) (43). We assess the central role of HIF-2α, which drives enhanced Sema3G expression by directly binding to the Sema3G promoter, thereby reducing neovascularization in the retinas of OIR mice. Therefore, the interplay of HIF-2α/Sema3G signaling further supports the broad role of Sema3G as a hypoxia-regulated protein and a crucial regulator of angiogenesis.

It is known that transmembrane holoreceptors constituted by neuropilins and plexins mediate the signal transduction of secreted semaphorins on vessels (9). In the present study, we reveal that endothelial Sema3G preserves microvascular integrity via Nrp2/PlexinD1 signaling. Prior findings indicated that PlexinD1 is dominantly expressed in ECs during cardiovascular development (53,

63), and PlexinD1 deficiency induces multiple cardiovascular defects (63, 64). We found that PlexinD1 deficiency abolishes the protective effect of Sema3G in vitro and in vivo, further supporting the importance of PlexinD1 in mediating the regression of pathological blood vessels and consequently the regrowth of functional vessels. Furthermore, vascular defects observed in *Cdh5-Cre Sema3G$^{fl/fl}$* OIR mice are similar to the previously reported phenotype of postnatal inactivation of the *PlexinD1* gene in OIR mice. The number of pathological extraretinal tufts were markedly increased in inducible inactivation of *PlexinD1* mice, and VEGF-mediated disoriented projections of filopodia could be suppressed by enhanced expression of PlexinD1 (65). Our results and those of another study indicate that Sema3G induces PlexinD1-mediated cellular responses in cells (17). Future work will aim to uncover the effect of Sema3G-PlexinD1 in regulating other retinal neovascular diseases.

Of particular importance is our finding that Sema3G is required for vascular stability in the retina during pathophysiological processes by protecting β-catenin from degradation. β-Catenin plays an essential role in developmental and homeostatic processes or pathology, which functions as a multifunctional intracellular protein (48, 66). Of note, it binds to VE-cadherins to protect them from degradation at cell-to-cell adherens junctions and stabilizes their interaction with the cytoskeleton (44–46). Our data illustrate that Sema3G-depleted ECs develop decreased β-catenin expression accompanied by reduced VE-cadherin stabilization at junctions. This impaired effect in ECs can be reversed by β-catenin overexpression or continuous activation of β-catenin signaling via an inhibitory effect on the degradation of β-catenin. These data are in agreement with the notion that postnatal retina lacking β-catenin in endothelial cells displays a reduction in vessel density, resulting in correspondingly premature vessel regression (34, 67). Meanwhile, Sema3G promotes vascular normalization in retinopathy, possibly through its role in the coordination of β-catenin–dependent vascular remodeling to increase vascular stability. The quantities of neovascular area and avascular area are interdependent, with the rate of revascularization being able to influence the regression of neovascularization (68). Our findings collectively suggest that endothelial Sema3G is required for the maturation of BRB and vascular remodeling by stabilizing the expression of β-catenin.

Our study provides the first in vivo demonstration of the physiological functions of Sema3G in vascular development using endothelial-specific *Sema3G* knockout mice and further reveals the protective effect of Sema3G in pathological cases using an OIR model. We demonstrate that the Sema3G-Nrp2/PlexinD1–β-catenin signaling axis functions as an essential defense mechanism deployed by the vasculature to reduce pathological angiogenesis and to promote the formation of a stable vascular network during ischemic retinopathy. Cumulatively, our study provides a novel insight into the mechanisms by which Sema3G regulates vascular stability and remodeling, especially at the phase of vascular regression in vasculopathy, encouraging further exploration of its therapeutic effects in the context of ischemic retinopathy treatment.

Methods

Additional information can be found in the Supplemental Methods.

Patient samples. All patients who were diagnosed with PDR or DME and underwent vitrectomy or intravitreal anti-VEGF drug injection were included. Vitreous samples were obtained from consenting patients who underwent vitrectomy surgery. The vitreous samples from the control group were collected from patients who underwent surgical treatment for nonvascular pathology (idiopathic epiretinal membrane [ERM] or idiopathic macular hole [MH]) by the same surgeon. The samples of vitreous were placed on ice immediately after biopsy and centrifuged at 4°C. The supernatants were collected, aliquoted into sterile tubes, and stored at –80°C. Fibrovascular membranes were excised from patients with severe PDR at the time of vitreoretinal surgery. Aqueous samples were obtained from consenting patients who underwent intravitreal anti-VEGF drug injection. Control aqueous samples were collected from patients without retinal vascular diseases and diabetes mellitus before undergoing cataract surgery. The samples of aqueous were immediately frozen on dry ice after collection and stored at –80°C.

Mice. *Sema3G$^{fl/fl}$* mice (12) were generated by introducing 2 loxP sites into introns flanking exons 2 to 4. To elucidate the role of Sema3G in ECs, *Sema3G$^{fl/fl}$* mice were intercrossed with *Cdh5-Cre* mice (RRID: IMSR_JAX: 006137, Jackson Laboratory). For comparison, we used *Sema3G$^{fl/fl}$* and EC-specific *Sema3G* homozygous-deficient (*Cdh5-Cre Sema3G$^{fl/fl}$*) littermates in the same experiments. *Cdh5-Cre* mice were crossed with *Ai14* mice (Rosa26-tdTomato Cre reporter line, RRID: IMSR_JAX: 007914, Jackson Laboratory) to confirm the specificity of Cre expression. Mice were housed in an air-conditioned room with a 12-hour light/dark cycle with free access to water and chow.

Assessment of protein levels by ELISA. Concentrations of Sema3G, IL-8, and VEGFA protein in human vitreous fluid were measured using a human semaphorin 3G ELISA kit (LSBio, LS-F19460), human IL-8 ELISA kit (Thermo Fisher Scientific, KHC0081), and a human VEGFA Mini Samples ELISA kit (Thermo Fisher Scientific, BMS277-2) according to the manufacturer's instructions.

RNA in situ hybridization. Detection of mRNA was performed in situ using the RNAscope reagent kit (Advanced Cell Diagnostics) following the manufacturer's instructions. Details can be found in the Supplemental Methods.

RT-qPCR. Total RNA extracted with RNAiso Plus (Takara) was reverse transcribed using a PrimeScript RT reagent kit (Perfect Real Time, Takara). RT-qPCR was carried out on a Bio-Rad CFX96 Touch Deep Well Real-Time PCR instrument using the SYBR Premix Ex Taq II (Takara), or on a QuantStudio 5 (Applied Biosystems) using AceQ qPCR SYBR Green Master Mix (Low ROX Premixed) (Vazyme, Q131-02). The primer sequences are listed in Supplemental Table 4. Relative gene expression was analyzed by $2^{-\Delta\Delta Ct}$ method and normalized to GAPDH.

RNA sequencing and data analysis. Sequencing was performed on an Illumina sequencer with a standard workflow. Details can be found in the Supplemental Methods. The data has been deposited at the NIH Sequence Read Archive under accession number PRJNA667618.

Immunostaining of whole-mount retinas. Flat-mount retina immunostaining was performed as previously described (30). To analyze and quantify the retina vascular phenotype, whole eyes from mice at P5, P6, P10, P14, P20, and P60 were collected and fixed in 4% PFA, respectively. After being washed in PBS, the retinas were dissected and blocked for 1 hour in blocking buffer and incubated overnight with IB4 and the primary antibodies. Subsequently, retinas were incubated with the appropriate fluorescently labeled secondary antibodies (Thermo Fisher Scientific, 1:500) for 2 hours at room temperature. After washes with washing buffer, retinas were flat-mounted on microscope slides. Images were acquired using a NikonA1R confocal microscope.

Analysis of postnatal retinal angiogenesis. All images shown are representative of the retinal vascular phenotype observed in at least 5 individual pups from 2 to 3 different litters in each group. Detailed quantifications can be found in the Supplemental Methods.

OIR mouse model. The procedure for the OIR model was carried out according to the methods previously described (19). To induce vaso-obliteration, mouse pups along with their nursing mothers were exposed to hyperoxia (75% oxygen) at P7 in an oxygen chamber. At P12, the pups were returned to normoxia (21% O_2). For mRNA analysis of *Sema3s* and *Vegfa*, age-matched mice housed in room air served as normoxic controls. Retinas of normoxic controls or OIR mice were harvested at P13, P17, P19, P21, or P25 for mRNA analysis. For analysis of retinal vaso-obliteration and neovascularization area, retinas of *Sema3G*$^{fl/fl}$ or *Cdh5-Cre Sema3G*$^{fl/fl}$ mice were harvested at P13, P15, P17, and P19. Detailed quantifications can be found in the Supplemental Methods. For LiCl rescue experiments, LiCl (50 mg/kg) or NaCl was injected i.p. once per day at P17 and P18, then retinas were harvested at P19 and processed for immunostaining. The phenotype of Sema3G knockout mice in the OIR model was compared with those of littermate controls. OIR mice in each group were only included if they consistently gained body weight (Supplemental Table 3). The mice with weight less than 6 g at P17 were excluded in OIR studies (19, 69).

Viral injection. To knockdown PlexinD1 in retinal vascular ECs, AAV-shControl or AAV-shPlexinD1 (7.0×10^{10} viral genome–containing particles/mouse) was injected into neonatal *Cdh5-Cre Sema3G*$^{fl/fl}$ mice at P7 and P12 through the retro-orbital sinus. To overexpress Sema3G in retinal vascular ECs, AAV-Control or AAV-Sema3G (7.0×10^{10} viral genome-containing particles/mouse) was injected into neonatal *Sema3G*$^{fl/fl}$ or *Cdh5-Cre Sema3G*$^{fl/fl}$ mice through the retro-orbital sinus at P7 and P12. These mice with their nursing mothers were exposed to 75% O_2 at P7 for 5 days, followed by normoxia. The retinas were analyzed at P19.

Intravitreal injections. To supply the retina with recombinant Sema3G at P15, pups were anesthetized using 2% isoflurane flowing through a face mask. During the experiment, a thermocontrolled heating pad was used to maintain body temperature. A quantity of 1 μg recombinant Sema3G or IgG protein was intravitreally injected to *Sema3G*$^{fl/fl}$ or *Cdh5Cre Sema3G*$^{fl/fl}$ mice using pulled glass micropipettes attached to a 10 μL Hamilton syringe. The eyes were treated with a triple antibiotic ointment after intravitreal injection. At P17, the retinas were harvested for analysis.

Statistics. We followed the standard sample sizes used in similar experiments in each of the relevant fields in the literature. All values were expressed as mean ± SEM. Comparisons between 2 experimental groups were made using the 2-tailed unpaired Student's *t* test. Statistical significance for differences among groups was tested by 1-way ANOVA with Tukey's multiple comparisons test, 1-way ANOVA with Dunnett's multiple comparisons test, or 2-way ANOVA with Bonferroni's multiple comparisons test. A P value less than 0.05 was considered significant. All the statistical analyses were performed using GraphPad Prism 6 (GraphPad Software).

Study approval. For mice, all procedures involving the use of animals were approved by the Institutional Animal Care and Use Committee of Zhejiang University and Nanjing Medical University. All surgery and human samples were harvested according to the principles outlined in the Declaration of Helsinki. Written informed consent was obtained from the patients. We obtained approval for the human clinical protocol from the Medical Research Ethics Committee United of the First Affiliated Hospital of Nanjing Medical University (Nanjing, China; Clinical Trial Registration: http://www.chictr.org.cn, unique identifier ChiCTR-IIR-17014160; http://www.clinicaltrials.gov, unique identifier NCT03506750).

Author contributions

DYC and NHS designed research studies, conducted experiments, and acquired and analyzed data. XC and JJG assisted with bioinformatics analysis. STY and ZZH performed all human surgeries. NNL, JK, and KF provided intellectual input or reagents. QHL, YML, and FH conceived the study, secured funding, and supervised the work. DYC and NHS wrote the manuscript with support from all other authors. The order of co–first authors was decided by discussions among the 2 first authors and the corresponding author.

Acknowledgments

The authors thank Alex L. Kolodkin from the Johns Hopkins University School of Medicine for providing us with AP-Sema3F, PlexinD1, and Nrp2 vectors. This work was supported by the State Key Program of National Natural Science Foundations of China (81730101 and 81930103 to FH) and the National Natural Science Foundations of China (81973300 to YML).

Address correspondence to: Ying-Mei Lu, Department of Physiology, School of Basic Medical Sciences, Nanjing Medical University, 101 Longmian Avenue, Jiangning District, Nanjing, 211166, China. Phone: 86.25.8686.9495; Email: lufx@njmu.edu.cn. Or to: Feng Han, Key Laboratory of Cardiovascular & Cerebrovascular Medicine, Drug Target and Drug Discovery Center, School of Pharmacy, Nanjing Medical University, 101 Longmian Avenue, Jiangning District, Nanjing, 211166, China. Phone: 86.25.8686.8462; Email: fenghan169@njmu.edu.cn. Or to: Qinghuai Liu, Department of Ophthalmology, The First Affiliated Hospital of Nanjing Medical University, 300 Guangzhou Road, Gulou District, Nanjing, 210029, China. Phone: 86.25.6830.3160; Email: liuqh@njmu.edu.cn.

1. Korn C, Augustin HG. Mechanisms of vessel pruning and regression. *Dev Cell*. 2015;34(1):5–17.
2. Mazzoni J, et al. The Wnt inhibitor Apcdd1 coordinates vascular remodeling and barrier maturation of retinal blood vessels. *Neuron*. 2017;96(5):1055–1069.
3. Antonetti DA, et al. Diabetic retinopathy. *N Engl J Med*. 2012;366(13):1227–1239.
4. Hellstrom A, et al. Retinopathy of prematurity. *Lancet*. 2013;382(9902):1445–1457.
5. Kim LA, D'Amore PA. A brief history of anti-VEGF for the treatment of ocular angiogenesis. *Am J Pathol*. 2012;181(2):376–379.
6. Mintz-Hittner HA, et al. Efficacy of intravitreal bevacizumab for stage 3+ retinopathy of prematurity. *N Engl J Med*. 2011;364(7):603–615.
7. Rodrigues EB, et al. Therapeutic monoclonal antibodies in ophthalmology. *Prog Retin Eye Res*. 2009;28(2):117–144.
8. Walchli T, et al. Wiring the vascular network with neural cues: a CNS perspective. *Neuron*. 2015;87(2):271–296.
9. Larrivee B, et al. Guidance of vascular development: lessons from the nervous system. *Circ Res*. 2009;104(4):428–441.
10. Sakurai A, et al. Semaphorin signaling in angiogenesis, lymphangiogenesis and cancer. *Cell Res*. 2012;22(1):23–32.
11. Kutschera S, et al. Differential endothelial transcriptomics identifies semaphorin 3G as a vascular class 3 semaphorin. *Arterioscler Thromb Vasc Biol*. 2011;31(1):151–159.
12. Tan C, et al. Endothelium-derived semaphorin

3G regulates hippocampal synaptic structure and plasticity via Neuropilin-2/PlexinA4. *Neuron*. 2019;101(5):920–937.
13. Liu M, et al. Mechanism of SEMA3G knockdown-mediated attenuation of high-fat diet-induced obesity. *J Endocrinol*. 2020;244(1):223–236.
14. Karayan-Tapon L, et al. Semaphorin, neuropilin and VEGF expression in glial tumours: SEMA3G, a prognostic marker? *Br J Cancer*. 2008;99(7):1153–1160.
15. Yoshikawa Y, et al. Frequent deletion of 3p21.1 region carrying semaphorin 3G and aberrant expression of the genes participating in semaphorin signaling in the epithelioid type of malignant mesothelioma cells. *Int J Oncol*. 2011;39(6):1365–1374.
16. Zhou X, et al. Effects of SEMA3G on migration and invasion of glioma cells. *Oncol Rep*. 2012;28(1):269–275.
17. Liu X, et al. Semaphorin 3G provides a repulsive guidance cue to lymphatic endothelial cells via Neuropilin-2/PlexinD1. *Cell Rep*. 2016;17(9):2299–2311.
18. Taniguchi M, et al. Identification and characterization of a novel member of murine semaphorin family. *Genes Cells*. 2005;10(8):785–792.
19. Connor KM, et al. Quantification of oxygen-induced retinopathy in the mouse: a model of vessel loss, vessel regrowth and pathological angiogenesis. *Nat Protoc*. 2009;4(11):1565–1573.
20. Joyal JS, et al. Ischemic neurons prevent vascular regeneration of neural tissue by secreting semaphorin 3A. *Blood*. 2011;117(22):6024–6035.
21. Oubaha M, et al. Senescence-associated secretory phenotype contributes to pathological angiogenesis in retinopathy. *Sci Transl Med*. 2016;8(362):362ra144.
22. Sun Y, et al. RORα modulates semaphorin 3E transcription and neurovascular interaction in pathological retinal angiogenesis. *FASEB J*. 2017;31(10):4492–4502.
23. Vanlandewijck M, et al. A molecular atlas of cell types and zonation in the brain vasculature. *Nature*. 2018;554(7693):475–480.
24. Russo RC, et al. The CXCL8/IL-8 chemokine family and its receptors in inflammatory diseases. *Expert Rev Clin Immunol*. 2014;10(5):593–619.
25. Apte RS, et al. VEGF in signaling and disease: beyond discovery and development. *Cell*. 2019;176(6):1248–1264.
26. Kubo Y, et al. Periostin and tenascin-C interaction promotes angiogenesis in ischemic proliferative retinopathy. *Sci Rep*. 2020;10(1):9299.
27. Urbancic M, et al. Correlations between vitreous cytokine levels and inflammatory cells in fibrovascular membranes of patients with proliferative diabetic retinopathy. *Mol Vis*. 2020;26:472–482.
28. Harada C, et al. The role of cytokines and trophic factors in epiretinal membranes: involvement of signal transduction in glial cells. *Prog Retin Eye Res*. 2006;25(2):149–164.
29. Alva JA, et al. VE-Cadherin-Cre-recombinase transgenic mouse: a tool for lineage analysis and gene deletion in endothelial cells. *Dev Dyn*. 2006;235(3):759–767.
30. Pitulescu ME, et al. Inducible gene targeting in the neonatal vasculature and analysis of retinal angiogenesis in mice. *Nat Protoc*. 2010;5(9):1518–1534.
31. Milde F, et al. The mouse retina in 3D: quantification of vascular growth and remodeling. *Integr Biol (Camb)*. 2013;5(12):1426–1438.
32. Birdsey GM, et al. The endothelial transcription factor ERG promotes vascular stability and growth through Wnt/β-catenin signaling. *Dev Cell*. 2015;32(1):82–96.
33. Fan J, et al. Crim1 maintains retinal vascular stability during development by regulating endothelial cell Vegfa autocrine signaling. *Development*. 2014;141(2):448–459.
34. Phng LK, et al. Nrarp coordinates endothelial Notch and Wnt signaling to control vessel density in angiogenesis. *Dev Cell*. 2009;16(1):70–82.
35. Chen DY, et al. GPR124 facilitates pericyte polarization and migration by regulating the formation of filopodia during ischemic injury. *Theranostics*. 2019;9(20):5937–5955.
36. Knowland D, et al. Stepwise recruitment of transcellular and paracellular pathways underlies blood-brain barrier breakdown in stroke. *Neuron*. 2014;82(3):603–617.
37. Lengfeld JE, et al. Endothelial Wnt/β-catenin signaling reduces immune cell infiltration in multiple sclerosis. *Proc Natl Acad Sci U S A*. 2017;114(7):E1168–E1177.
38. Liebner S, et al. Functional morphology of the blood-brain barrier in health and disease. *Acta Neuropathol*. 2018;135(3):311–336.
39. Chow BW, Gu C. Gradual suppression of transcytosis governs functional blood-retinal barrier formation. *Neuron*. 2017;93(6):1325–1333.
40. Lee J, et al. Angiopoietin-1 guides directional angiogenesis through integrin αvβ5 signaling for recovery of ischemic retinopathy. *Sci Transl Med*. 2013;5(203):203ra127.
41. Xin X, et al. Hypoxic retinal Muller cells promote vascular permeability by HIF-1-dependent up-regulation of angiopoietin-like 4. *Proc Natl Acad Sci U S A*. 2013;110(36):3425–3434.
42. Krock BL, et al. Hypoxia-induced angiogenesis: good and evil. *Genes Cancer*. 2011;2(12):1117–1133.
43. Hu CJ, et al. Differential roles of hypoxia-inducible factor 1alpha (HIF-1alpha) and HIF-2alpha in hypoxic gene regulation. *Mol Cell Biol*. 2003;23(24):9361–9374.
44. McCrea PD, Gottardi CJ. Beyond β-catenin: prospects for a larger catenin network in the nucleus. *Nat Rev Mol Cell Biol*. 2016;17(1):55–64.
45. Nelson WJ, Nusse R. Convergence of Wnt, beta-catenin, and cadherin pathways. *Science*. 2004;303(5663):1483–1487.
46. Bienz M. beta-Catenin: a pivot between cell adhesion and Wnt signalling. *Curr Biol*. 2005;15(2):R64–R67.
47. Lilien J, Balsamo J. The regulation of cadherin-mediated adhesion by tyrosine phosphorylation/dephosphorylation of beta-catenin. *Curr Opin Cell Biol*. 2005;17(5):459–465.
48. MacDonald BT, et al. Wnt/beta-catenin signaling: components, mechanisms, and diseases. *Dev Cell*. 2009;17(1):9–26.
49. Tran KA, et al. Endothelial β-catenin signaling is required for maintaining adult blood-brain barrier integrity and central nervous system homeostasis. *Circulation*. 2016;133(2):177–186.
50. Wickline ED, et al. Hepatocyte γ-catenin compensates for conditionally deleted β-catenin at adherens junctions. *J Hepatol*. 2011;55(6):1256–1262.
51. Uhl FE, et al. Preclinical validation and imaging of Wnt-induced repair in human 3D lung tissue cultures. *Eur Respir J*. 2015;46(4):1150–1166.
52. Hedgepeth CM, et al. Activation of the Wnt signaling pathway: a molecular mechanism for lithium action. *Dev Biol*. 1997;185(1):82–91.
53. Gu C, et al. Semaphorin 3E and plexin-D1 control vascular pattern independently of neuropilins. *Science*. 2005;307(5707):265–268.
54. Wang Q, et al. Neuropilin-2/PlexinA3 receptors associate with GluA1 and mediate Sema3F-dependent homeostatic scaling in cortical neurons. *Neuron*. 2017;96(5):1084–1098.
55. Korbelin J, et al. A brain microvasculature endothelial cell-specific viral vector with the potential to treat neurovascular and neurological diseases. *EMBO Mol Med*. 2016;8(6):609–625.
56. Grossniklaus HE, et al. Animal models of choroidal and retinal neovascularization. *Prog Retin Eye Res*. 2010;29(6):500–519.
57. Lambert V, et al. Laser-induced choroidal neovascularization model to study age-related macular degeneration in mice. *Nat Protoc*. 2013;8(11):2197–2211.
58. Ragauskas S, et al. In vivo multimodal imaging and analysis of mouse laser-induced choroidal neovascularization model. *J Vis Exp*. 2018;(131):56173.
59. Huang X, et al. Genome editing abrogates angiogenesis in vivo. *Nat Commun*. 2017;8(1):112.
60. Klagsbrun M. Mediators of angiogenesis: the biological significance of basic fibroblast growth factor (bFGF)-heparin and heparan sulfate interactions. *Semin Cancer Biol*. 1992;3(2):81–87.
61. Heinolainen K, et al. VEGFR3 modulates vascular permeability by controlling VEGF/VEGFR2 signaling. *Circ Res*. 2017;120(9):1414–1425.
62. Witmer AN, et al. Vascular endothelial growth factors and angiogenesis in eye disease. *Prog Retin Eye Res*. 2003;22(1):1–29.
63. Gitler AD, et al. PlexinD1 and semaphorin signaling are required in endothelial cells for cardiovascular development. *Dev Cell*. 2004;7(1):107–116.
64. Zhang Y, et al. Tie2Cre-mediated inactivation of plexinD1 results in congenital heart, vascular and skeletal defects. *Dev Biol*. 2009;325(1):82–93.
65. Fukushima Y, et al. Sema3E-PlexinD1 signaling selectively suppresses disoriented angiogenesis in ischemic retinopathy in mice. *J Clin Invest*. 2011;121(5):1974–1985.
66. Dejana E. The role of wnt signaling in physiological and pathological angiogenesis. *Circ Res*. 2010;107(8):943–952.
67. Wang Y, et al. Norrin/Frizzled4 signaling in retinal vascular development and blood brain barrier plasticity. *Cell*. 2012;151(6):1332–1344.
68. Stahl A, et al. The mouse retina as an angiogenesis model. *Invest Ophthalmol Vis Sci*. 2010;51(6):2813–2826.
69. Stahl A, et al. Postnatal weight gain modifies severity and functional outcome of oxygen-induced proliferative retinopathy. *Am J Pathol*. 2010;177(6):2715–2723.